

HETEROGENEOUS MAGNETIC SUPERCONDUCTING SYSTEMS

SERKAN ERDIN

School of Physics and Astronomy
University of Minnesota, Minneapolis, MN 55455, USA.

I. INTRODUCTION

Heterogeneous magnetic superconducting systems (HMSS) represent a new class of nanostructures. They are made of ferromagnetic (FM) and superconducting (SC) pieces separated by thin layers of insulating oxides. In contrast to the case of a homogeneous ferromagnetic superconductor studied during the last two decades, the two order parameters, the magnetization and the SC electron density do not suppress each other [1, 2]. In HMSS, the interaction between the two order parameters is due to the magnetic field created by the magnetic and SC textures. Strong interaction of the FM and SC systems not only gives rise to a new class of novel phenomena and physical effects, but also shows the important technological promise of devices whose transport properties can be easily tuned by comparatively weak magnetic fields.

The interplay between ferromagnetism and superconductivity has long been the focus of studies both experimental and theoretical [3, 4, 5, 6]. In 1957, Ginzburg pointed out [7] that the two phenomena can occur in thin films and wires, due to the small FM induction and relatively large SC critical fields. Afterwards, Anderson and Suhl [8] described the conditions for both phenomena to appear simultaneously in the bulk. The domain-like magnetic structure in the coexistence phase was noted independently by two different groups [9, 10]. Later, Suhl developed the detailed version of the Landau-Ginzburg theory of ferromagnetic superconductors [11], e.g. HoMo_6S_8 and ErRh_4B_4 . The first experiment in this context was carried out by Mathias *et al.* [12]. The coexistence of ferromagnetism and superconductivity in the bulk has been observed recently in the cuprates $\text{RuSr}_2\text{GdCu}_2\text{O}_{8-\gamma}$ [13] and $\text{RuSr}_2\text{Gd}_{1+x}\text{Ce}_{1-x}\text{Cu}_2\text{O}_{10}$ [14, 15] below their SC transition temperatures $T_s = 15 - 40$ K and $T_s = 37$ K (for $x = 0.2$) respectively. It is possible to avoid the mutual suppression of the FM and SC order parameters by separating them in space [1]. Such structures can be made with modern nanofabrication techniques. The proximity effect and spin diffusion which suppress both order parameters can be easily avoided by growing a thin insulating oxide layer between the FM and SC components. Several theoretical studies have proposed different possibilities for realization of HMSS: arrays of magnetic dots on the top of a SC film [1, 16], single magnetic dot of various geometries on top of a SC film [17, 18, 19], ferromagnetic/superconducting bilayers (FSB) and multilayers (FSM) [20, 21, 22, 23], magnetic nanorods embedded into a superconductor [24, 25] and semi-infinite HMSS [26].

In HMSS, the strong interaction between FM and SC components stems from the magnetic fields generated by the inhomogeneous magnetization and the supercurrents as well as SC vortices. SC vortices were widely studied, both experimentally and theoretically, in the literature

[28]. Vortices in SC films were first studied by J. Pearl [29]. He realized that their current decays in space more slowly than those in the bulk.

Similar models of HMSS were studied theoretically by other groups in different configurations. Marmorkos *et al.* investigated the giant vortex state created by a magnetic dot, of size on the order of the coherence length ξ , embedded in a SC film by solving the nonlinear Landau-Ginzburg equations [17]. Kayali [18, 19] and Peeters *et al.* [30] studied vortex creation by both in-plane and out-of-plane magnetized ferromagnets of different shapes on a SC thin film. Sasik and Santos *et al.* considered an array of FM dots on a SC film [31, 32]. They treated the dots as magnetic dipoles, ignoring their real geometry and showed that they excite and pin SC vortices. Carneiro studied interaction between vortices in SC films and magnetic dipole arrays, and showed that the arrays with antiferromagnetic order is more effective in vortex creation than the arrays with ferromagnetic order [33]. Symmetry violation in SC thin films with regular arrays of magnetic dots are reported by two different studies [16, 34]. Bulaevskii *et al.* discussed the pinning of vortices in ferromagnet-superconductor multilayers [35]. The same group also examined the effect of the screening magnetic field on a thick magnetic layer which is placed on top of a bulk superconductor [36]. They found that the magnetic domains shrink in the presence of the SC film. In the most of theoretical studies, hard magnets are considered. Recently, Helseth found that identical vortices can attract each other in the presence of soft magnets [37].

To date, only sub-micron magnetic dots covered by thin SC films have been prepared and studied [38, 39, 40, 41, 42, 43, 44]. The experimental samples of FM-SC hybrid systems were prepared by means of electron beam lithography and lift-off techniques [45]. Both in-plane and out-of-plane magnetization was experimentally studied. The dots with magnetization parallel to the plane were fabricated from Co, Ni, Fe, Gd-Co and Sm-Co alloys. For the dots with magnetization perpendicular to the plane, Co/Pt multilayers were used. The FM dots were deposited on thin SC films made of either Nb or Pb, whose transition temperatures are around 7 – 10 K. In these experiments, the effect of commensurability on the transport properties (e.g. magnetoresistance oscillations and matching anomalies) was observed. However, this effect is not limited to the magnets interacting with superconductors and was first found many years ago by Martinoli and his group [46]. They studied the transport properties of SC films with periodically modulated thickness in an external magnetic field. They found oscillations of critical current versus magnetic field. Recently, several experimental groups observed commensurability effects caused by a periodic array of magnetic dots or holes [47, 48, 49, 50]. These results confirm that the FM dots create and pin vortices. However, much more interesting and promising would be effects specific for the HMSS, which are associated with the violation of the time reversal symmetry. Some of them include spontaneous currents in the ground state [24, 51, 52, 53]. So far only one such effect was experimentally observed: an asymmetry of the SC hysteresis in the presence of magnetic dots [39].

In HMSS, the magnetic field induced by inhomogeneous magnetization penetrates into a superconductor through SC vortices, while the magnetic field generated by the supercurrents and SC vortices acts on the magnetic system. The mutual interaction between FM and SC subsystems offer interesting physical effects such as spontaneous symmetry violation [16], shrinkage of FM domains and a magnetic domain wall [21, 36, 54], SC transition temperature shift [23] and Bean-Livingstone-like energy barrier for vortices [26].

We recently developed a method based on London-Maxwell equations to study theoretical realizations of HMSS [27]. In this article, we first review this method and its extension to periodic systems and finite systems. Next, some of our recent results on a SC film with a FM

dot grown upon it and domain structures in FSB and further studies in these systems are briefly discussed. This review is prepared as a progress report and aims to give reader the basic aspects of HMSS. This article is organized as follows: In the next section, a method to calculate inhomogeneous magnetization and supercurrents including SC vortices in the London approximation is presented with great details. In section II, a FM dot on top of a SC film and vortex states in the ground state are discussed. Section III is devoted to the recent theoretical results on FSB. We conclude with discussions and summary in section IV. To help reader follow easily the theoretical analysis in this chapter, we give details of calculations with Bessel functions and series in the appendices.

II. THEORY

In both theoretically proposed and experimentally realized HMSS, the magnetic texture interacts with the superconducting (SC) current. An inhomogeneous magnetization generates a magnetic field outside the magnets that in turn generates screening currents in the superconductor, which subsequently change the magnetic field. The problem must be solved self-consistently. In the literature, HMSS have been studied through Landau-Ginzburg equations [17] and linear London method. Though the SC vortices are treated more accurately in the former in which SC electron density n_s changes in the vicinity of the vortex core, solving non-linear Landau-Ginzburg equations is numerically difficult. In London approach, n_s is assumed to be constant, and vortices are treated as points. However, London's approximation is sufficient when the sizes of all the structures in the problem greatly exceed the coherence length ξ , and offers more analytical insight. For this reason, we have been studying the several realizations of HMSS through a method based on London-Maxwell equations. Here we present the method to calculate inhomogeneous magnetization and supercurrents including the SC vortices in the London approximation. In the next section a method for the most general 3-dimensional HMSS is given. In section B, this method is applied to the case of very thin ferromagnetic (FM) and SC films. In section C, the method is extended to periodic heterogeneous magnetic superconducting systems (PHMSS). In the last section, we show how this method can be applied to semi-infinite and finite systems.

A. Three Dimensional Systems

The total energy of a stationary FM-SC system reads [55]

$$U = \int \left[\frac{\mathbf{B}^2}{8\pi} + \frac{m_s n_s \mathbf{v}_s^2}{2} - \mathbf{B} \cdot \mathbf{M} \right] dV. \quad (1)$$

where \mathbf{B} is the magnetic induction, \mathbf{M} is the magnetization, n_s is the density of SC electrons, m_s is their effective mass and \mathbf{v}_s is their velocity. We assume the SC density n_s and the magnetization \mathbf{M} to be separated in space. We also assume that the magnetic field \mathbf{B} and its vector-potential \mathbf{A} asymptotically approaches zero at infinity. After the static Maxwell equation $\nabla \times \mathbf{B} = \frac{4\pi}{c} \mathbf{j}$, and $\mathbf{B} = \nabla \times \mathbf{A}$ are employed, the magnetic field energy can be transformed as follows:

$$\int \frac{\mathbf{B}^2}{8\pi} dV = \int \frac{\mathbf{j} \cdot \mathbf{A}}{2c} dV. \quad (2)$$

Although the vector potential enters explicitly in the last equation, it is gauge invariant due to current conservation $\text{div} \mathbf{j} = 0$. When integrating by parts, we neglect the surface term. This approximation is correct if the field, vector potential and current decrease sufficiently fast at infinity. The current \mathbf{j} can be represented as a sum: $\mathbf{j} = \mathbf{j}_s + \mathbf{j}_m$ of the SC and magnetic currents, respectively [56]:

$$\mathbf{j}_s = \frac{n_s \hbar e}{2m_s} (\nabla \phi - \frac{2\pi}{\phi_0} \mathbf{A}), \quad (3)$$

$$\mathbf{j}_m = c \nabla \times \mathbf{M}. \quad (4)$$

where $\phi_0 = hc/2e$ is the SC flux quantum. We separately consider the contributions from magnetic and SC currents to the integral (2), starting with the integral:

$$\frac{1}{2c} \int \mathbf{j}_m \cdot \mathbf{A} dV = \frac{1}{2} \int (\nabla \times \mathbf{M}) \cdot \mathbf{A} dV. \quad (5)$$

Integrating by parts and neglecting the surface term again, we arrive at

$$\frac{1}{2c} \int \mathbf{j}_m \cdot \mathbf{A} dV = \frac{1}{2} \int \mathbf{M} \cdot \mathbf{B} dV. \quad (6)$$

We have omitted the integral over a distant surface:

$$\oint (\mathbf{n} \times \mathbf{M}) \cdot \mathbf{A} dS. \quad (7)$$

Such an omission is justified if the magnetization is confined to a limited volume. But for infinite magnetic systems it may be wrong even in the simplest problems.

We next consider the contribution of the SC current \mathbf{j}_s to the integral (2). In the gauge-invariant Eq.(3), ϕ is the phase of the SC carriers wave-function. Note that the phase gradient $\nabla \phi$ can be incorporated in \mathbf{A} as a gauge transformation. The exception is vortex lines, where ϕ is singular. We use the equation (3) to express the vector potential \mathbf{A} in terms of the supercurrent and the phase gradient:

$$\mathbf{A} = \frac{\phi_0}{2\pi} \nabla \phi - \frac{m_s c}{n_s e^2} \mathbf{j}_s. \quad (8)$$

Plugging Eq.(8) into Eq.(2), we find

$$\frac{1}{2c} \int \mathbf{j}_s \cdot \mathbf{A} dV = \frac{\hbar}{4e} \int \nabla \phi \cdot \mathbf{j}_s dV - \frac{m_s}{2n_s e^2} \int j_s^2 dV. \quad (9)$$

Since the superconducting current is

$$\mathbf{j}_s = en_s \mathbf{v}_s. \quad (10)$$

The last term in Eq.(9) equals the negative of the kinetic energy and thus exactly compensates the kinetic energy in the initial expression for the energy (1). Collecting all the remaining terms, we obtain the following expression for the total energy:

$$U = \int \left[\frac{n_s \hbar^2}{8m_s} (\nabla \phi)^2 - \frac{n_s \hbar e}{4m_s c} \nabla \phi \cdot \mathbf{A} - \frac{\mathbf{B} \cdot \mathbf{M}}{2} \right] dV. \quad (11)$$

This expression is complete except for a possible surface term for infinite magnetic systems. Note that integration volume includes both superconductors and magnets. Eq. (11) allows us to separate the energy of the vortices, the energy of magnetization and the energy of their interaction. Indeed, as we noted earlier, the phase gradient can be ascribed to the contribution of vortex lines alone. It can be represented as a sum of independent integrals over distinct vortex lines. The vector-potential and the magnetic field can also be presented as a sum of magnetization induced and vortex induced parts: $\mathbf{A} = \mathbf{A}_m + \mathbf{A}_v$, $\mathbf{B} = \mathbf{B}_m + \mathbf{B}_v$, where \mathbf{A}_k , \mathbf{B}_k (the index k is either m or v) are determined as solutions of the London-Maxwell equations generated by the magnetization and the vortices. The effect of the SC screening of the magnetic field due to the magnetization is already included in the vector fields \mathbf{A}_m and \mathbf{B}_m . If such separation of fields is applied, then the total energy, (11) becomes a sum of terms containing vortex contributions alone, magnetic contributions alone and the interaction terms. The purely magnetic component can be represented as a non-local quadratic form of the magnetization. The purely superconducting part becomes a non-local double integral over the vortex lines. Finally, the interaction term may be presented as a double integral over the vortex lines and the volume occupied by the magnetization, and is bi-linear in magnetization and vorticity.

B. Two Dimensional Textures and Vortices

Below we show a detailed analysis in the case of parallel FM and SC films, both very thin and positioned close to each other. Neglecting their thickness, we assume both films to be located approximately at $z = 0$. In some cases we need a higher degree of accuracy. We then introduce a small distance d between the films, which in the end approaches zero. Although the thickness of each film is assumed to be small, the 2-dimensional densities of super-carriers $n_s^{(2)} = n_s d_s$ and magnetization $\mathbf{m} = \mathbf{M} d_m$ remain finite. Here d_s is the thickness of the SC film and d_m is the thickness of the FM film. The 3d super-carrier density in the SC film is $n_s(\mathbf{R}) = \delta(z) n_s^{(2)}(\mathbf{r})$ and the 3d magnetization in the FM film is $\mathbf{M}(\mathbf{R}) = \delta(z - d) \mathbf{m}(\mathbf{r})$, where \mathbf{r} is the two-dimensional radius-vector and the z -direction is chosen to be perpendicular to the films. In what follows the 2d SC density $n_s^{(2)}$ is assumed to be a constant and the index (2) is omitted. The energy (11) for this special case takes the following form:

$$U = \int \left[\frac{n_s \hbar^2}{8m_s} (\nabla\varphi)^2 - \frac{n_s \hbar e}{4m_s c} \nabla\varphi \cdot \mathbf{a} - \frac{\mathbf{b} \cdot \mathbf{m}}{2} \right] d^2 \mathbf{r}, \quad (12)$$

where $\mathbf{a} = \mathbf{A}(\mathbf{r}, z = 0)$ and $\mathbf{b} = \mathbf{B}(\mathbf{r}, z = 0)$. The vector potential satisfies the Maxwell-London equation, which is derived from the static Maxwell equation $\nabla \times \mathbf{B} = \frac{4\pi}{c} \mathbf{j}$, where \mathbf{j} is the total current density on the surface of the superconductor, and is given by $\mathbf{j} = (\mathbf{j}_s + \mathbf{j}_m) \delta(z)$. The supercurrent and the magnetic current densities are given in Eqs.(3, 4). Using $\mathbf{B} = \nabla \times \mathbf{A}$, the Maxwell-London equation reads

$$\nabla \times (\nabla \times \mathbf{A}) = -\frac{1}{\lambda} \mathbf{A} \delta(z) + \frac{2\pi \hbar n_s e}{m_s c} \nabla\varphi \delta(z) + 4\pi \nabla \times (\mathbf{m} \delta(z)). \quad (13)$$

Here $\lambda = \lambda_L^2 / d_s$ is the effective screening length for the SC film, and $\lambda_L = \left(\frac{m_s c^2}{4\pi n_s e^2} \right)^{\frac{1}{2}}$ is the London penetration depth [57].

According to our general arguments, the term proportional to $\nabla\varphi$ in Eq. (13) describes vortices. A plane vortex characterized by its vorticity n and by the position \mathbf{r}_0 of its center on the plane, contributes a singular term to $\nabla\varphi$:

$$\nabla\varphi_0(\mathbf{r}, \mathbf{r}_0) = n \frac{\hat{z} \times (\mathbf{r} - \mathbf{r}_0)}{|\mathbf{r} - \mathbf{r}_0|^2}, \quad (14)$$

and generates a Pearl vortex vector potential(see Appendix A for details):

$$\mathbf{A}_{v0}(\mathbf{r} - \mathbf{r}_0, z) = \frac{n\phi_0}{2\pi} \frac{\hat{z} \times (\mathbf{r} - \mathbf{r}_0)}{|\mathbf{r} - \mathbf{r}_0|} \int_0^\infty \frac{J_1(q|\mathbf{r} - \mathbf{r}_0|)e^{-q|z|}}{1 + 2\lambda q} dq, \quad (15)$$

where $J_1(x)$ is Bessel function of the first order. Different vortices contribute independently in the vector potential and magnetic field. In the limit of zero film thickness, the usual Coulomb gauge, $\text{div}\mathbf{A} = 0$, leads to strong singularity in the vector potential, due to the surface currents in the SC and FM films, which leads to the discontinuity at $z = 0$. Therefore, we choose to employ another gauge $A_z = 0$. The calculations become simple in the Fourier-representation. Following the previous section, we write the Fourier transform of the vector potential $\mathbf{A}_{\mathbf{k}}$ as a sum $\mathbf{A}_{\mathbf{k}} = \mathbf{A}_{m\mathbf{k}} + \mathbf{A}_{v\mathbf{k}}$ of independent contributions from magnetization and vortices. Using the following definitions of the Fourier transform:

$$\mathbf{A}_{\mathbf{k}} = \int \mathbf{A}(\mathbf{r}, z) e^{-i\mathbf{q}\cdot\mathbf{r} - ik_z z} d^3r, \quad (16)$$

$$\mathbf{a}_{\mathbf{q}} = \int \mathbf{a}(\mathbf{r}, z=0) e^{-i\mathbf{q}\cdot\mathbf{r}} d^2r. \quad (17)$$

The equation for the magnetic part of the vector-potential reads

$$\mathbf{k}(\mathbf{k} \cdot \mathbf{A}_{m\mathbf{k}}) - k^2 \mathbf{A}_{m\mathbf{k}} = \frac{\mathbf{a}_{m\mathbf{q}}}{\lambda} - 4\pi i \mathbf{k} \times \mathbf{m}_{\mathbf{q}} e^{ik_z d}, \quad (18)$$

where \mathbf{q} is the projection of the wave vector \mathbf{k} onto the plane of the films: $\mathbf{k} = k_z \hat{z} + \mathbf{q}$. An arbitrary vector field $\mathbf{V}_{\mathbf{k}}$ in wave-vector space can be fixed by its coordinates in a local frame of reference formed by the vectors $\hat{z}, \hat{q}, \hat{z} \times \hat{q}$:

$$\mathbf{V}_{\mathbf{k}} = V_{\mathbf{k}}^z \hat{z} + V_{\mathbf{k}}^{\parallel} \hat{q} + V_{\mathbf{k}}^{\perp} (\hat{z} \times \hat{q}). \quad (19)$$

The solution to equation (18) with $A_z = 0$ is found by taking the inner product of equation (19) with \hat{q}, \hat{z} and $\hat{z} \times \hat{q}$, respectively as below:

$$A_{m\mathbf{k}}^{\parallel} = -\frac{4\pi i m_{\mathbf{q}}^{\perp}}{k_z} e^{ik_z d} - \frac{a_{m\mathbf{q}}^{\parallel}}{k_z^2 \lambda}, \quad (20)$$

$$A_{m\mathbf{k}}^{\perp} = -\frac{4\pi i m_{\mathbf{q}}^{\perp}}{k_z} e^{ik_z d}, \quad (21)$$

$$A_{m\mathbf{k}}^z = -\frac{1}{\lambda k^2} a_{\mathbf{q}}^z + \frac{4\pi i (k_z m_{\mathbf{q}}^{\parallel} - q m_{\mathbf{q}z})}{k^2} e^{ik_z d}. \quad (22)$$

Integration of the latter equation over k_z gives the perpendicular component of $\mathbf{a}_{\mathbf{q}}^{(m)}$:

$$a_{m\mathbf{q}}^\perp = -\frac{4\pi\lambda q(m_{\mathbf{q}}^\parallel + im_{\mathbf{q}z})}{1 + 2\lambda q} e^{-qd}. \quad (23)$$

It follows from Eqs.(20, 21) that $a_{m\mathbf{q}}^\parallel = 0$. Note that Eq. (21) for the parallel component of the vector potential $A_{m\mathbf{k}}^\parallel$ does not contain any information on the SC film. This component corresponds to zero magnetic field outside the FM film. Therefore, it is not essential for our problem. The vortex part of the vector potential $\mathbf{A}_{v\mathbf{k}}$ also has not a z -component since the supercurrents flow in the plane. The vortex-induced vector potential is [57]

$$\mathbf{A}_{v\mathbf{k}} = \frac{2i\phi_0(\hat{q} \times \hat{z})F(\mathbf{q})}{\mathbf{k}^2(1 + 2\lambda q)}, \quad (24)$$

where $F(\mathbf{q}) = \sum_j n_j e^{i\mathbf{q} \cdot \mathbf{r}_j}$ is the vortex form-factor; the index j labels the vortices, n_j denotes the vorticity of the j th vortex and \mathbf{r}_j are coordinates of the vortex centers. The Fourier-transform of the vortex-induced vector potential at the surface of the SC film $\mathbf{a}_{v\mathbf{q}}$ reads

$$\mathbf{a}_{v\mathbf{q}} = \frac{i\phi_0(\hat{q} \times \hat{z})F(\mathbf{q})}{q(1 + 2\lambda q)}. \quad (25)$$

We express the energy (12) in terms of the fields and vector-potential Fourier-transforms separating the purely magnetic, purely vortex and the interaction parts:

$$U = U_{vv} + U_{mm} + U_{mv}. \quad (26)$$

The vortex energy U_{vv} is the same as it would be in the absence of the FM film:

$$U_{vv} = \frac{n\hbar^2}{8m_s} \int \nabla\varphi_{-\mathbf{q}} \cdot \left(\nabla\varphi_{\mathbf{q}} - \frac{2\pi}{\phi_0} \mathbf{a}_{v\mathbf{q}} \right) \frac{d^2q}{(2\pi)^2} \quad (27)$$

However, the magnetic energy U_{mm} :

$$U_{mm} = -\frac{1}{2} \int \mathbf{m}_{-\mathbf{q}} \cdot \mathbf{b}_{m\mathbf{q}} \frac{d^2q}{2\pi^2} \quad (28)$$

contains the screened magnetic field \mathbf{b} and therefore differs from its value in the absence of the SC film, but it does not depend on the vortex positions. The interaction energy reads

$$\begin{aligned} U_{mv} &= -\frac{n\hbar e}{4m_s c} \int (\nabla\varphi)_{-\mathbf{q}} \cdot \mathbf{a}_{m\mathbf{q}} \frac{d^2q}{(2\pi)^2} \\ &\quad - \frac{1}{2} \int \mathbf{m}_{-\mathbf{q}} \cdot \mathbf{b}_{v\mathbf{q}} \frac{d^2q}{(2\pi)^2}. \end{aligned} \quad (29)$$

Note that only the form-factor $F(\mathbf{q})$ conveys any information about the vortex arrangement.

C. Periodic Systems

A periodic heterogeneous magnetic superconducting system (PHMSS) such as a magnetic dot array or a periodic domains in ferromagnet-superconductor bilayers can be studied with the method described in the previous section. However, it is necessary to modify the equations given above for the periodic structures of interest. In this section, we extend the above method to study PHMSSs. In doing so, we still assume that PHMSSs are made of very thin magnetic textures with the magnetization perpendicular to the plane and SC films. Their energy is calculated over the surface of the SC film. We start with the energy of the 2d systems (12). In the plane of the PHMSS, the magnetic field \mathbf{b} , the magnetization \mathbf{m} , the phase gradient $\nabla\varphi$ and the vector potential \mathbf{a} are 2d periodic functions. Therefore, we need to express them in terms of Fourier series. For any function $f(\mathbf{r})$, the Fourier expansion is given by

$$\mathbf{f}(\mathbf{r}) = \sum_{\mathbf{G}} \mathbf{f}_{\mathbf{G}} e^{i\mathbf{G}\cdot\mathbf{r}} \quad \mathbf{f}_{\mathbf{G}} = \frac{1}{\mathcal{A}} \int \mathbf{f}(\mathbf{r}) e^{-i\mathbf{G}\cdot\mathbf{r}} d^2\mathbf{r}. \quad (30)$$

The \mathbf{G} s are the reciprocal vectors of the periodic structure of interest, and \mathcal{A} is the elementary cell area. We first express \mathbf{a} , \mathbf{b} , \mathbf{m} and $\nabla\varphi$ in terms of the Fourier series as in (30), then substitute them back in (12). Performing the integral over the infinite area of the 2d system and using $\int e^{i(\mathbf{G}+\mathbf{G}')\cdot\mathbf{r}} d^2r = \mathcal{A}\delta_{\mathbf{G},-\mathbf{G}'}$, we obtain the energy per unit cell u for the 2d PHMSS expressed in terms of Fourier components as follows:

$$u = \sum_{\mathbf{G}} \left[\frac{n\hbar^2}{8m_s} |(\nabla\varphi)_{\mathbf{G}}|^2 - \frac{n\hbar e}{4m_s c} (\nabla\varphi)_{\mathbf{G}} \cdot \mathbf{a}_{-\mathbf{G}} - \frac{\mathbf{b}_{\mathbf{G}} \cdot \mathbf{m}_{-\mathbf{G}}}{2} \right]. \quad (31)$$

The Fourier coefficients of the vector potentials, \mathbf{a}_m and \mathbf{a}_v for both the magnetic part and the vortices in terms of continuous Fourier vectors are already given in (23) and (25). They can be rewritten in terms of reciprocal vectors as

$$\mathbf{a}_{m\mathbf{G}} = \frac{4\pi\lambda i\mathbf{G} \times \hat{z} m_z \mathbf{G}}{1 + 2\lambda G}, \quad (32)$$

$$\mathbf{a}_{v\mathbf{G}} = \frac{i\phi_0(\hat{G} \times \hat{z})F_{\mathbf{G}}}{\mathcal{A}G(1 + 2\lambda G)}. \quad (33)$$

Using the Fourier coefficients of the magnetic field and the phase gradient:

$$\mathbf{b}_{\mathbf{G}} = i\mathbf{G} \times \mathbf{a}_{\mathbf{G}}, \quad (34)$$

$$(\nabla\varphi)_{\mathbf{G}} = 2\pi i(\mathbf{G} \times \hat{z} F_{\mathbf{G}})/(\mathcal{A}G^2), \quad (35)$$

and replacing the vector potentials in (31) by (32) and (33), the energy of the PHMSS per unit cell is found term by term as

$$u_{vv} = \frac{\phi_0^2}{4\pi\mathcal{A}^2} \sum_{\mathbf{G}} \frac{|F_{\mathbf{G}}|^2}{G(1 + 2\lambda G)}, \quad (36)$$

$$u_{mv} = -\frac{\phi_0}{\mathcal{A}} \sum_{\mathbf{G}} \frac{m_z \mathbf{G} F_{-\mathbf{G}}}{1 + 2\lambda G}, \quad (37)$$

$$u_{mm} = -2\pi\lambda \sum_{\mathbf{G}} \frac{G^2 |\mathbf{m}_z \mathbf{G}|^2}{1 + 2\lambda G}. \quad (38)$$

D. Finite Systems

In the most of theoretical studies, SC subsystem is considered to be infinite size for the sake of computational simplicity. Although it is relatively hard to handle SC system's boundaries in both Landau-Ginzburg and London equations, several groups have studied finite or semi-finite realizations of HMSS. We recently considered semi-infinite HMSS elsewhere [26], by benefiting from the ideas of Kogan's study of Pearl vortex near the edge of SC film[58]. Here, we propose an alternative method to treat semi-infinite and finite realizations of HMSS. To this end, we modify London-Maxwell equation (see Eq.(13)). The boundary condition can be incorporated into Maxwell-London equation by using step function, namely supercurrent is zero outside the SC system's boundary. Together with step function, Maxwell-London equation reads

$$\nabla \times \nabla \times \mathbf{A} = \frac{4\pi}{c}(\mathbf{j}_s\theta(\mathbf{r}' - \mathbf{r}) + \mathbf{j}_m), \quad (39)$$

where $\mathbf{j}_s = \frac{c\Phi_0}{8\pi^2\lambda}\nabla\phi - \frac{c}{4\pi\lambda}\mathbf{a}$ and $\theta(\mathbf{r}' - \mathbf{r})$ is step function that equals 0 or 1 when \mathbf{r} is greater than the boundary's position \mathbf{r}' or otherwise. For semi-infinite system in which 2-d SC film lies on x-y plane and its edge is located at x=0, step function is $\theta(x)$. For a finite circular SC disk of radius R, step function becomes $\theta(R - r)$. Eq.(39) can be solved by similar techniques used in the previous sections, however its solution gives rather complicated integral equations. We leave the details of the solution to further works.

III. FM DOT ON SC FILM

In this section, we review the studies related to the ground state of a superconducting (SC) film in the presence of a circular FM dot grown upon it (see (see Fig. 1)). In this case, the magnetization is assumed to be fixed and homogeneous within the dot, and directed perpendicular to the SC film. This problem is previously discussed elsewhere [27], in which we predicted the geometrical pattern formed by vortices in the ground state. Here, we give further details of analysis and some new results. The problems we discuss are: i) under what conditions do vortices appear in the ground state; ii) where they appear, and iii) the magnetic fields and currents in these states. As in the previous section, we assume the SC film to be a very thin plane, and infinite in the lateral directions. Since the magnetization is confined within the finite dot, no integrals over infinitely remote surfaces or contours arise. In the next section, we treat the first case using the method described in the previous chapter.

Let both SC and FM films be infinitely thin and placed at heights $z = 0$ and $z = d$, respectively. The SC film is infinite in lateral directions, whereas the FM film is finite and has the shape of circle with radius R (magnetic dot). The 2d magnetization of the magnetic dot is $\mathbf{m}(\mathbf{r}) = m\hat{z}\sigma(R - r)\delta(z - d)$, where $\sigma(x)$ is the step function, equal to +1 for $x > 0$ and 0 for $x < 0$. We first find the vector potential and magnetic field induced by the dot in the presence of the SC film, using Eqs. (22,23). The Fourier-component ofd at magnetization necessary for this calculation is

$$\mathbf{m}_{\mathbf{k}} = \hat{z}\frac{2\pi mR}{q}J_1(qR)e^{ik_z d}, \quad (40)$$

where $J_1(x)$ is the Bessel function. From (25) with (40), the calculations employ Fourier-

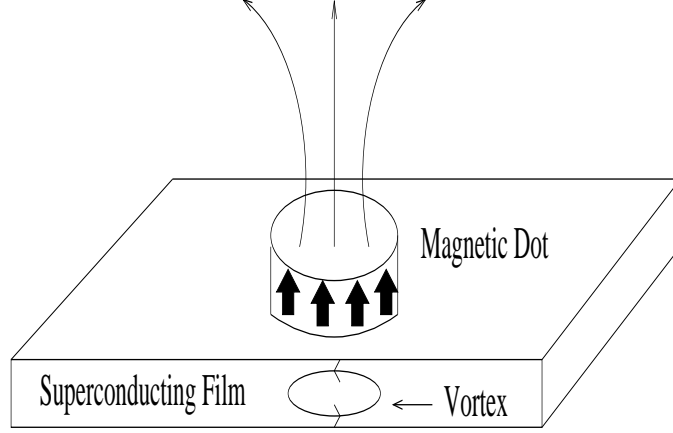


FIG. 1: Magnetic dot on a superconducting film.

transform of the vector potential at the superconductor surface:

$$a_{m\mathbf{q}}^{\perp} = -\frac{i8\pi^2\lambda mR}{1+2\lambda q}J_1(qR). \quad (41)$$

In the last equation we have replaced e^{-qd} by 1. The Fourier-transform of the vector potential reads

$$A_{m\mathbf{k}}^{\perp} = -\frac{i8\pi^2mRJ_1(qR)}{k^2} \left[e^{-qd} \frac{2q\lambda}{1+2\lambda q} + (e^{ik_z d} - e^{-qd}) \right]. \quad (42)$$

Though the difference in the round brackets in equation (42) appears to be small (recall that d must be set to zero in the final answer), we cannot neglect it since it implies a finite, not small discontinuity in the parallel component of magnetic field at the two film faces. From equation (42) we can immediately find the Fourier-transforms of the magnetic field components via

$$B_{m\mathbf{k}}^z = iqA_{m\mathbf{k}}^{\perp}; \quad B_{m\mathbf{k}}^{\perp} = -ik_z A_{m\mathbf{k}}^{\perp}. \quad (43)$$

The inverse Fourier-transformation of Eqs. (43,42) gives the magnetic field in real space:

$$B_m^z(\mathbf{r}, z) = 4\pi\lambda mR \int_0^{\infty} \frac{J_1(qR)J_0(qr)e^{-q|z|}}{1+2\lambda q} q^2 dq, \quad (44)$$

$$B_m^r(\mathbf{r}, z) = -2\pi mR \int_0^{\infty} J_1(qR)J_1(qr)e^{-q|z|} \left[\frac{2q\lambda}{1+2\lambda q} \text{sign}(z) + \text{sign}(z-d) - \text{sign}(z) \right] q dq, \quad (45)$$

where $\text{sign}(z)$ is the function equal to the sign of its argument. Note that B_m^r has discontinuities at $z = 0$ and $z = d$ due to surface currents in the SC and FM films respectively; whereas, the normal component B_m^z is continuous.

Symmetry arguments imply that a vortex, if it appears, must be located at the center of the dot. Indeed, for $R \gg \lambda$, an analytical calculation shows that the central position of the vortex provides minimal energy. We have checked numerically that the central position is always energy favorable for one vortex. This fact is not trivial since the magnetic field of the dot is stronger near its boundary and a violation of symmetry could be naively expected. However, the gain of energy due to interaction of the magnetic field generated by the vortex with the magnetization of the dot decreases when the vortex approaches the boundary.

Another interesting problem is the sign of the perpendicular component of the magnetic field. The vector potential generated by a vortex is given by Eq. (24) with $F(\mathbf{q}) = 1$. The perpendicular component of the magnetic field generated by the vortex is

$$B_v^z = \frac{\phi_0}{2\pi} \int_0^\infty \frac{J_0(qr)e^{-q|z|}}{1 + 2\lambda q} q dq. \quad (46)$$

Numerical calculation based on Eqs. (44, 46) shows that, in the presence of the vortex centered at $r = 0$, B_z on the SC film ($z = 0$) changes sign for some $r > R$ (see Fig. 2), but it is negative for all $r > R$ without the vortex. The physical explanation of this fact is as follows. The dot

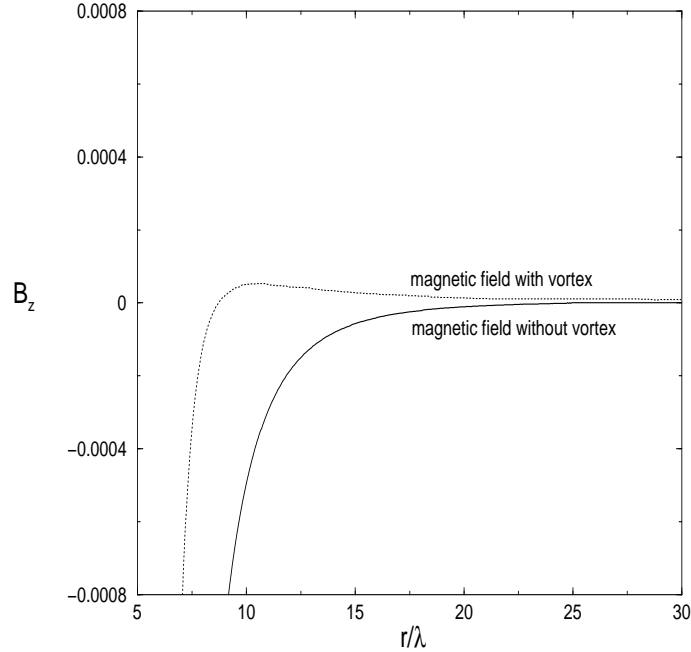


FIG. 2: Magnetic field of a dot with and without vortex for $R/\lambda = 5$ and $\phi_0/8\pi^2 mR = 0.05$.

itself is an ensemble of parallel magnetic dipoles. Each dipole generates a magnetic field whose z -component on the plane passing through the dot has sign opposite to the dipolar moment. However, the field exactly over and under the dipole has the same sign as the dipole and is strongly singular. The fields from different dipoles compete at $r < R$, but they have the same

sign at $r > R$. The SC current tends to screen the magnetic field of the magnetic dot and have the opposite sign. The field generated by a vortex at large distances decays more slowly than the screened dipolar field ($1/r^3$ vs. $1/r^5$). Thus, the sign of B_z is opposite to the magnetization at small values of r (but larger than R) and positive at large r . Measurement of the magnetic field near the film may serve as a diagnostic tool to detect a SC vortex bound by the dot. To our knowledge, so far there are no experimental measurements of this effect.

The energy of the system in the presence of many vortices with arbitrary vorticities n_i can be calculated using Eqs.(26-29). The appearance of N vortices with arbitrary positions \mathbf{r}_i in the system changes the energy by an amount:

$$\Delta_N = \sum_{i=1}^N n_i^2 \epsilon_v + \frac{1}{2} \sum_{i \neq j}^N n_i n_j \epsilon_{vv}(r_{ij}) + \sum_{i=1}^N n_i \epsilon_{mv}(r_i). \quad (47)$$

Here $\epsilon_v = \epsilon_0 \ln(\lambda/\xi)$ is the energy of a vortex without a magnetic dot, $\epsilon_0 = \phi_0^2/(16\pi^2\lambda)$ and ϵ_{vv} is the vortex-vortex interaction and ϵ_{mv} is the vortex-magnetic dot interaction. Substituting (25) into the vortex energy ϵ_{vv} of (27), we get

$$\epsilon_{vv}(r_{ij}) = \frac{\epsilon_0}{\pi} \left[H_0\left(\frac{r_{ij}}{2\lambda}\right) - Y_0\left(\frac{r_{ij}}{2\lambda}\right) \right], \quad (48)$$

where $r_{ij} = |\mathbf{r}_j - \mathbf{r}_i|$, $H_0(x)$ and $Y_0(x)$ are the Struve function of the zeroth order and the modified Bessel function of the second kind of the zeroth order, respectively [59]. For ϵ_{mv} of (29), direct substitution of the vector potential, magnetic field and the phase gradient (see Eqs. (41,44)) into (29) gives

$$\epsilon_{mv}(r_i) = -m\phi_0 R \int_0^\infty \frac{J_1(qR)J_0(qr_i)dq}{1+2\lambda q}. \quad (49)$$

In order for N vortices to appear, the necessary condition is that $\Delta_N < 0$ and $\Delta_N < \Delta_{N-1}$. Using this criteria, we can determine in what configurations and order the vortices appear. To this end, we study only vortices with positive vorticity which are situated under the dot. Under the assumption that the dot's diameter is larger than ξ , it is reasonable to think that vortices with multiple vorticities, the so-called giant vortices, do not appear, since the vortex energy grows as the square of its vorticity (see Eq.(47)). For large dots $R \gg \lambda$ and sufficiently small m , the giant vortex is definitely energy unfavorable. However for $R < \lambda$ and $mR \gg \phi_0$, it can be favorable. This question has not yet been analyzed completely.

The next step is to minimize (47) with respect to the positions of the vortices. We first start with one vortex. It turns out that it appears at the center of the dot. Δ_1 is a function of two dimensionless variables $m\phi_0/\epsilon_v$ and R/λ . $\Delta_1 = 0$ defines a critical curve separating regions with and without vortices, and is depicted in Fig. 3. Stability occurs ($\Delta_N < 0$) for the regions in Fig. 3 below the critical curves. The asymptotic behavior of ϵ_{mv} for large and small values of R/λ can be found analytically (see Appendix C for details):

$$\epsilon_{mv} \approx -m\phi_0 \quad \left(\frac{R}{\lambda} \gg 1\right), \quad (50)$$

$$\epsilon_{mv} \approx -m\phi_0 \frac{R}{2\lambda} \quad \left(\frac{R}{\lambda} \ll 1\right). \quad (51)$$

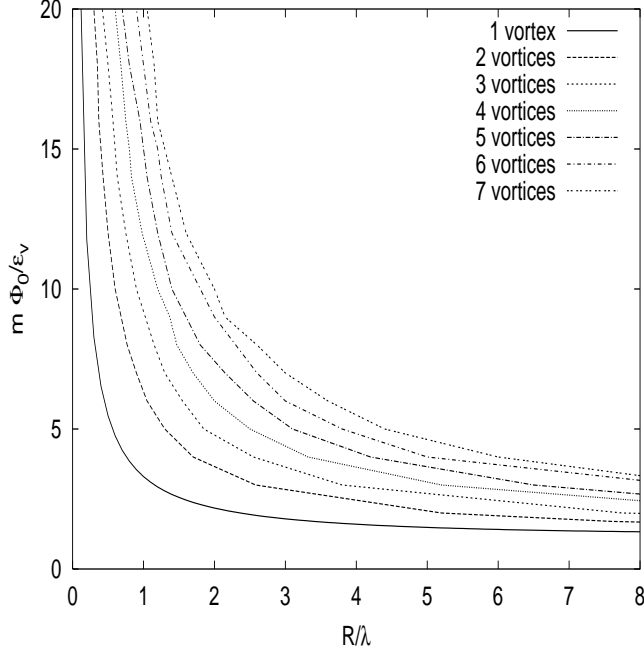


FIG. 3: Magnetic dot on a superconducting film.

Thus, asymptotically the curve $\Delta_1 = 0$ turns into a horizontal straight line $m\phi_0/\epsilon_v = 1$ at large R/λ and into a logarithmically distorted hyperbola $(m\phi_0/\epsilon_v)(R/\lambda) = 2$ at small R/λ .

For further increase of either $m\phi_0/\epsilon_v$ or R/λ , the second vortex becomes energetically favorable. Due to symmetry, the centers of the two vortices are located on a straight line connecting the vortices with the center of the dot at equal distances from the center. The curve 2 on Fig. 3 corresponds to this second phase transition. The occurrence of 2 vortices can be experimentally detected as the violation of circular symmetry of the field. For three vortices, the equilibrium configuration is a regular triangle. The further increase of $m\phi_0/\epsilon_v$ or R/λ makes other vortex states more energetically favorable. In principle there exists an infinite series of such transitions. Here, we limit ourselves to the first seven transitions by considering the next four vortex states. In equilibrium, for vortices sit on the corners of a square, whereas five vortices form a pentagon. We find that geometrical pattern for six vortices is hexagon. For the case of seven vortices, equilibrium configuration is different from the first six states. Namely, one vortex is situated at the dot's center, while other six vortices form a hexagonal shape (see Fig.4).

It is not yet clear what is the role of configurations with several vortices confined within the dot region and antivortices outside. Note that these results are valid for infinite systems. When the FM dot is placed on top of a finite SC film, we suspect that the geometrical patterns formed by vortices will be quite different. To investigate this hypothesis, we recently studied the FM dot on a semi-infinite SC film, and found that the vortex is shifted either towards or away from the SC film's boundary due to the competition between the attraction of a vortex with the SC film's edge via its image vortex and the interaction between the dot and the vortex [26].

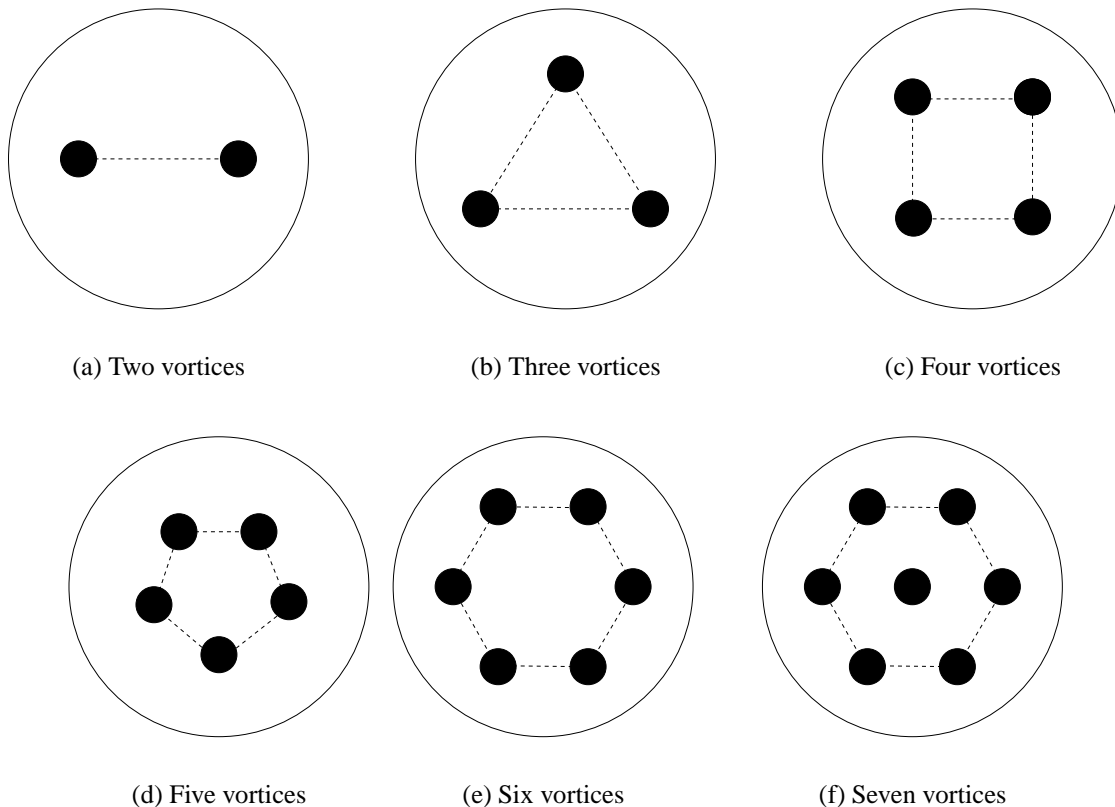


FIG. 4: Vortex states

IV. FERROMAGNETIC-SUPERCONDUCTING BILAYERS

Earlier Lyuksyutov and Pokrovsky noticed [20, 53] that in a bilayer consisting of homogeneous superconducting (SC) and ferromagnetic (FM) films with the magnetization normal to the plane, SC vortices occur spontaneously in the ground state, even though the magnet does not generate a magnetic field in the SC film. In previous work [21], we presented a theory of such vortex-generation instability and the resulting vortex structures, and showed that that due to this instability, domains with alternating magnetization and vortex directions occur in ferromagnetic-superconducting bilayers (FSB). In this chapter, we review the theory of FSB and the domain structures. In the next section, we treat these domain structures in the continuum regime in which the domain size is much larger than the effective penetration depth. This approximation does not work when the equilibrium size of the domains is on the order of the effective penetration depth. However, it can be recovered by considering the discrete lattice of vortices instead. In the second section, we report our preliminary results on the possible equilibrium structure in the discrete case and calculate the vortex positions, which depend on the magnetization and domain wall energy [60].

A. The Continuum Regime

We start by refining previous arguments establishing a topological instability in the FSB [20, 53]. We assume that the magnetic anisotropy is strong enough to keep the magnetization exactly perpendicular to the film (in the z -direction). The homogeneous FM film creates no magnetic field outside itself and hence does not alter the state of the SC film. The magnetic field generated by a single vortex in the superconducting film, with magnetic flux $\phi_0 = hc/2e$, interacts with the magnetization \mathbf{m} of the FM film and lowers the total energy by $-m\phi_0$ for a proper sign of vorticity. The energy to create a Pearl vortex in an isolated SC film is $\varepsilon_v = \varepsilon_0 \ln(\lambda/\xi)$ [29], where $\varepsilon_0 = \phi_0^2/16\pi^2\lambda$, $\lambda = \lambda_L^2/d$ is the effective penetration depth [57], λ_L is the London penetration depth, and ξ is the coherence length. Thus, the total energy of a single vortex in the FSB is

$$\varepsilon_v^{eff} = \varepsilon_v - m\phi_0, \quad (52)$$

and the FSB becomes unstable with respect to spontaneous formation vortices as soon as ε_v^{eff} turns negative. Note that close enough to the SC transition temperature T_s , ε_v^{eff} is definitely negative since the SC electron density n_s and, therefore, ε_v is zero at T_s (Recall that $\varepsilon_v(T) = \varepsilon_v(T=0)(1 - \frac{T^2}{T_s^2})$). For small m value, $\varepsilon_v^{eff} > 0$ at $T = 0$, the instability exists in the temperature interval $T_v < T < T_s$, where $\varepsilon_v^{eff}(T_v) = 0$, otherwise instability persists until $T = 0$.

A newly appearing vortex phase cannot consist only of vortices of one sign. Indeed, any system with average vortex density n_v would generate a constant magnetic field $B_z = n_v\phi_0$ along the z direction. The energy of this field for a finite film of the linear size L_f grows as L_f^3 , which quickly exceeds the gain in energy due to creation of vortices, proportional to L_f^2 . Hence, in order for the vortex array to survive, the film should split in domains with alternating magnetization and vortex directions. We show below that if the domain size L is much greater than the effective penetration length λ , the most favorable arrangement is the stripe domain structure. To this end we write the total energy of the bilayer in the form

$$U = U_{sv} + U_{vv} + U_{mv} + U_{mm} + U_{dw}, \quad (53)$$

where U_{sv} is the effective energy of single vortices; U_{vv} is the vortex-vortex interaction energy; U_{mv} is the energy of interaction between the vortices and magnetic field generated by domain walls; U_{mm} is the self-interaction energy of the magnetic layer; and U_{dw} is the linear tension energy of magnetic domain walls [60]. We assume that the 2d periodic domain structure consist of two equivalent sublattices, so that the magnetization $m_z(\mathbf{r})$ and density of vortices $n(\mathbf{r})$ alternate when crossing from one sublattice to another. The magnetization is assumed to have a constant absolute value: $m_z(\mathbf{r}) = ms(\mathbf{r})$, where $s(\mathbf{r})$ is the periodic step function equal to $+1$ at one sublattice and -1 at the other one. We consider a dilute vortex system where the vortex spacing is much larger than λ . Then the effective single-vortex energy becomes

$$U_{sv} = \varepsilon_v^{eff} \int n(\mathbf{r})s(\mathbf{r})d^2x. \quad (54)$$

Note that $n(\mathbf{r})s(\mathbf{r}) > 0$ in all cases. Due to ‘‘average neutrality’’ of the periodic stripe system, the energy of a single vortex in equation (54) is different from (52) : $\varepsilon_v^{eff} = \varepsilon_v - m\phi_0/2$. Note that, $-\frac{1}{2} \int \mathbf{b}^v \cdot \mathbf{m} d^2x$ term in Eq.(29) contributes $-m\phi_0/2$ in the effective single-vortex energy. In

the periodic systems, the contribution of the surface term is zero. The vortex-vortex interaction energy is

$$U_{vv} = \frac{1}{2} \int n(\mathbf{r})V(\mathbf{r}-\mathbf{r}')n(\mathbf{r}')d^2xd^2x', \quad (55)$$

where $V(\mathbf{r}-\mathbf{r}')$ is the pair interaction energy between vortices located at points \mathbf{r} and \mathbf{r}' . Its asymptotic value at large distances $|\mathbf{r}-\mathbf{r}'| \gg \lambda$ is [55]

$$V(\mathbf{r}-\mathbf{r}') = \frac{\Phi_0^2}{4\pi^2 |\mathbf{r}-\mathbf{r}'|}. \quad (56)$$

This long-range interaction is induced by the magnetic field generated by the Pearl vortices and their slowly decaying currents. By Eq.(29), the energy of the vortex interaction with the magnetic field generated by the magnetic film is [27]

$$U_{mv} = -\frac{\Phi_0}{16\pi^2\lambda} \int \nabla\varphi(\mathbf{r}-\mathbf{r}')n(\mathbf{r}') \cdot \mathbf{a}^{(m)}(\mathbf{r})d^2xd^2x'. \quad (57)$$

Here $\varphi(\mathbf{r}-\mathbf{r}') = \arctan \frac{y-y'}{x-x'}$ is a phase shift created at a point \mathbf{r} by a vortex centered at a point \mathbf{r}' and $\mathbf{a}^{(m)}(\mathbf{r})$ is the value of the vector-potential induced by the FM film upon the SC one. By Eq.(28), the magnetic self-interaction reads

$$U_{mm} = -\frac{m}{2} \int B_z^{(m)}(\mathbf{r})s(\mathbf{r})d^2x. \quad (58)$$

Finally, each magnetic domain wall's linear energy is $U_{dw} = \epsilon_{dw}L_{dw}$, where ϵ_{dw} is the linear tension of the magnetic domain wall and L_{dw} is the total length of the magnetic domain walls. Let us analyze the vortex-domain-wall interaction U_{mv} . The magnetic vector-potential $\mathbf{A}^{(m)}$ obeys the London-Pearl magneto-static equation (see Eq.(13)):

$$\nabla \times \left(\nabla \times \mathbf{A}^{(m)} \right) = \left[-\frac{1}{\lambda} \mathbf{a}^{(m)} + 4\pi \nabla \times (\hat{z}m(\mathbf{r})) \right] \delta(z). \quad (59)$$

We consider $L \gg \lambda$, where the term $\nabla \times \left(\nabla \times \mathbf{A}^{(m)} \right)$ is negligible and then

$$\mathbf{a}^{(m)} \approx -4\pi m \lambda \hat{z} \times \nabla s(\mathbf{r}). \quad (60)$$

The phase gradient entering Eq. (57) can be rewritten as: $\nabla\varphi(\mathbf{r}) = \hat{z} \times \nabla \ln |\mathbf{r}-\mathbf{r}'|$. Plugging this expression into (57), integrating by part and employing relation $\nabla^2 \ln |\mathbf{r}-\mathbf{r}'| = -2\pi\delta(\mathbf{r}-\mathbf{r}')$, we arrive at

$$U_{mv} = -\frac{\Phi_0}{2} \int m(\mathbf{r})n(\mathbf{r})d^2x. \quad (61)$$

This result implies that the vortex-domain-wall interaction renormalizes the single-vortex to

$$\tilde{\epsilon}_v = \epsilon_v - m\Phi_0. \quad (62)$$

Thus, the term U_{mv} can be removed from the total energy (53) if the single-vortex contribution U_{sv} is replaced by \tilde{U}_v , which differs from (54) on replacing ϵ_v^{eff} by $\tilde{\epsilon}_v$. In physical terms,

it means that the vortex attraction to the magnetic domain walls lowers the threshold for the spontaneous appearance of the vortex-domain structure. The next step is the minimization of energy with respect to $n(\mathbf{r})$ the vortex density, which appears only in the first three terms of the total energy (see Eq.(53)). Their sum can be conveniently denoted by $U_v \equiv \tilde{U}_{sv} + U_{vv}$. To simplify the minimization, we Fourier-expand the periodic functions: $s(\mathbf{r}) = \sum_{\mathbf{G}} s_{\mathbf{G}} e^{i\mathbf{G}\cdot\mathbf{r}}$ and $n(\mathbf{r}) = \sum_{\mathbf{G}} n_{\mathbf{G}} e^{i\mathbf{G}\cdot\mathbf{r}}$. The energy U_v in the Fourier-representation then reads

$$U_v = U_{sv} + U_{vv} + U_{mv} = \sum_{\mathbf{G}} \left(\tilde{\epsilon}_v s_{\mathbf{G}} n_{-\mathbf{G}} + \frac{1}{2} V_{\mathbf{G}} n_{\mathbf{G}} n_{-\mathbf{G}} \right), \quad (63)$$

where $V_{\mathbf{G}} = \int V(\mathbf{r}) e^{i\mathbf{G}\cdot\mathbf{r}} d^2x = \phi_0^2 / 2\pi |\mathbf{G}|$. Minimization of Eq.(63) over $n_{\mathbf{G}}$ leads to

$$n_{\mathbf{G}} = -\frac{\tilde{\epsilon}_v s_{\mathbf{G}}}{V_{\mathbf{G}}} = -\frac{2\pi \tilde{\epsilon}_v |\mathbf{G}| s_{\mathbf{G}}}{\phi_0^2}, \quad (64)$$

$$U_v = -\frac{\pi \tilde{\epsilon}_v^2}{\phi_0^2} \sum_{\mathbf{G}} |\mathbf{G}| |s_{\mathbf{G}}|^2. \quad (65)$$

Note that the solution becomes physically meaningless at positive $\tilde{\epsilon}_v$. We now apply these general results to analyze the stripe domain structure. In this case the density of vortices $n(x)$ depends only on one coordinate x perpendicular to the magnetic domain walls. The vectors \mathbf{G} are directed along the x -axis. The allowed wave numbers are $G = \pi(2r + 1)/L$, where L is the domain width and r runs over all integers. The Fourier-transform of the step function is $s_G = \frac{2i}{\pi(2r+1)}$. The inverse Fourier-transform of Eq. (64) for the stripe domain case is (see Appendix C for details)

$$n(x) = -\frac{4\pi \tilde{\epsilon}_v}{\phi_0^2 L} \frac{1}{\sin \frac{\pi x}{L}}. \quad (66)$$

Note the strong singularity of the density near the domain walls. Our approximation is invalid at distances of the order of λ , and the singularities must be smeared out in a band of the width λ around the magnetic domain wall. Conversely, the approximation of the zero-width magnetic domain wall is invalid within the range of the magnetic domain wall width l . Fortunately, we do not need more detailed information on the distribution of vortices in the vicinity of the magnetic domain walls. Indeed, by substituting the Fourier-transform of the step function into equation (65), we find a logarithmically divergent series in the form of $\sum_r 1/(2r + 1)$. It must be cut off at $\pm r_{max}$ with $r_{max} \sim L/\lambda$. The summation can be performed using the Euler asymptotic formula [65] with the following result (see Appendix C for details):

$$U_v^{str} = -\frac{4\tilde{m}^2 \mathcal{A}}{L} \left(\ln \frac{L}{\lambda} + C + 2 \ln 2 \right), \quad (67)$$

where $\tilde{m} = m - \epsilon_v/\phi_0$, \mathcal{A} is the domain area and $C \sim 0.577$. Now the problem is to analyze the proper cut-off for any lattice. As we have seen in the stripe domain structure, the energy U_v diverges logarithmically due to the strong singularity of the vortex density near each magnetic domain wall (see Eq. (66)). Thus, the logarithmic term is proportional to the total magnetic domain wall length (see Eq.(67)). The singularity of the vortex density contributes the similar logarithmic term to the energy for any lattice. However, this logarithmic accuracy is not sufficient to distinguish the domain structures. In order to solve this problem, we need the next

approximation to the energy U_v , i.e. a term α , proportional to the length of the magnetic domain wall, without the logarithmic factor. Together with this term, the energy for any lattice looks like $U_v \sim \ln(L\alpha/\lambda)$. Now, the problem is to find this term accurately. Such a term includes a non-local contribution from large distances between λ and L and a local contribution from the vicinity of the magnetic domain walls. The non-local contribution is accurately accounted for by the summation over the integers; whereas, the local contribution requires a cut-off at large r , which is not well defined. However, due to its local character it must be the same for all magnetic domain walls. Therefore, it is possible to choose the maximal wave-vector in the direction normal to the magnetic domain wall as $2\pi/\lambda$. Such a procedure renormalizes the magnetic domain wall's linear tension, in the same for any domain lattice. This remark allows calculation of the energy U_v for the square and triangular lattices. For the square checkerboard lattice, the allowed wave-vectors are $\mathbf{G} = \frac{\pi}{L} [(2r+1)\hat{x} + (2s+1)\hat{y}]$. The Fourier-transform of the step function is: $s_{\mathbf{G}} = \frac{4}{\pi^2(2r+1)(2s+1)}$. The maximal values of r and s are identical and equal to L/λ where L is the side of a square domain. The summation, similar to the case of stripe structure although somewhat more complicated, leads to the following expression (see Appendix C for details):

$$U_v^{sq} = -\frac{8\tilde{m}^2 \mathcal{A}}{L} \left(\ln \frac{L}{\lambda} + C + 2 \ln 2 - \gamma \right), \quad (68)$$

where the numerical constant γ is defined below:

$$\gamma = (2 - \sqrt{2}) \frac{7}{\pi^2} \zeta(3) + \frac{16}{\pi^2} \sum_{r=0}^{\infty} \sum_{s=r+1}^{\infty} \mathcal{S}(r, s). \quad (69)$$

Here $\zeta(x)$ is the Riemann zeta-function; $\zeta(3) \approx 1.2020$ and,

$$\mathcal{S}(r, s) = \frac{2(r+s+1) - \sqrt{(2r+1)^2 + (2s+1)^2}}{(2r+1)^2(2s+1)^2}. \quad (70)$$

Direct numerical calculation gives $\gamma \approx 0.9 > \ln 2$.

The reciprocal lattice vectors for the regular triangular domain lattice are $\mathbf{G} = \frac{2\pi}{L} \left[r \left(\hat{x} - \frac{1}{\sqrt{3}} \hat{y} \right) + s \frac{2}{\sqrt{3}} \hat{y} \right]$. The analysis is remarkably simplified in the ‘‘triangular coordinate frame’’: $u = x - y/\sqrt{3}$; $v = 2y/\sqrt{3}$. The step function inside one elementary cell is $s(u, v) = +1$ for $u + v < L$ and $s(u, v) = -1$ for $u + v > L$, where L is the side of the elementary triangle. The Fourier-transform of the step function $s_{\mathbf{G}}$ is not zero at either $r \neq 0, s = 0$, or $r = 0, s \neq 0$, or $r = s \neq 0$. For all these cases $|s_{\mathbf{G}}|^2 = 1/(\pi^2 q^2)$, where q is either r or s , depending on which of these numbers differs from zero. For this case, the summation in equation (65) gives

$$U_v^{tri} = -\frac{32\tilde{m}^2 \mathcal{A}}{L\sqrt{3}} (\ln r_{\max} + C). \quad (71)$$

However, the value r_{\max} is different from the stripe and square cases since the coordinates are skewed, here it equals $\frac{\sqrt{3}}{2} \frac{L}{\lambda}$.

Our next step is to show that the magnetization self-interaction can be included into the renormalized magnetic domain wall linear tension. For the isolated FM stripe domain structure, the magnetization self-interaction energy is equal to $U_{mm} = -m^2 L_{dw} \ln \frac{L}{l}$, where l is the

magnetic domain wall width [61, 62, 63]. The superconducting screening enhances the magnetic field very near the magnetic domain walls and reduces it way from the magnetic domain walls. In the stripe geometry, from Eq.(60), $b_z^{(m)} = da^{(m)}/dx = -4\pi m\lambda(d^2s/dx^2)$ implying that the screened magnetic field is confined to an interval $\sim \lambda$ near magnetic domain walls. Thus, its contribution to the energy does not contain a large logarithm. By (58), U_{mm} gives $-L_{dw}m^2$, which can be incorporated into the renormalized value of the magnetic domain wall linear tension. Note that this contribution is negative. We assume that it is less than the initial positive linear tension ϵ_{dw} . We do not consider here the interesting but less likely possibility of a negative renormalized linear tension, which probably results in domain wall branching.

Now we are in position to minimize the total energy U over the domain width L and compare the equilibrium energy. The equilibrium domain width and the equilibrium energy for the stripe structure are

$$L_{eq}^{(str)} = \frac{\lambda}{4} \exp\left(\frac{\epsilon_{dw}}{4\tilde{m}^2} - C + 1\right), \quad (72)$$

$$U_{eq}^{(str)} = -\frac{16\tilde{m}^2\mathcal{A}}{\lambda} \exp\left(-\frac{\epsilon_{dw}}{4\tilde{m}^2} + C - 1\right). \quad (73)$$

Calculating the corresponding values for the square and triangular lattice, we obtain: $L_{eq}^{(sq)} = L_{eq}^{(str)} \exp(\gamma)$; $U_{eq}^{(sq)} = 2U_{eq}^{(str)} \exp(-\gamma)$; and $U_{eq}^{(tri)} = (3/4)U_{eq}^{(str)}$. Comparing these energies to the energy of the stripe structure, for which $U_{eq}^{(str)} < 0$, we conclude that the stripe structure wins. The domains become infinitely wide at $T = T_s$ and at $T = T_v$. The expression in the exponent (73) at $T = T_s$ is four times less than the corresponding expression for domains in an isolated magnetic film [56]. Therefore, stripe domains in the bilayer can be energetically favorable even if the isolated magnetic film remains in a monodomain state. If stripe domains in the magnetic film exist above the SC transition, then they shrink dramatically below the transition. The physical reason behind this effect is as follows. There are two contributions to the energy that determines the domain width; magnetic energy and the domain wall energy. While the latter contribution prefers the larger domain width, the former contribution causes the smaller width. In the presence of superconductor, the magnetic field is screened due to the Meissner effect, which makes the magnetic energy contribution dominant. As a result, the domain width is smaller than that in the case of ferromagnet only. Bulaevsky and Chudnovsky [36] found that the domain width in a *thick* magnetic layer above a *bulk* superconductor is proportional to $d_m^{1/3}$ instead of $d_m^{1/2}$, a well-known result for an isolated magnetic layer. Here d_m is the thickness of the magnetic layer; "thick" means that $d_m \gg l$. Our problem is fundamentally different on two counts: first, we consider a *thin* FM film $d_m \ll l$ above a *thin* SC film and, second, the main effect is due to the interaction of vortices with the magnetization rather than from the screening of the magnetic field as in [36]. The vortex-magnetization interaction effect is much stronger, leading to a totally different dependence.

B. The Discrete Regime

If $\epsilon_{dw} \leq 4\tilde{m}^2$, the continuum approximation becomes invalid, since L_{eq} becomes on the order of or less than λ (see Eq.(72)). Instead a lattice of discrete vortices must be considered. In this section, we present a method which works in both continuum and the discrete regimes. We study

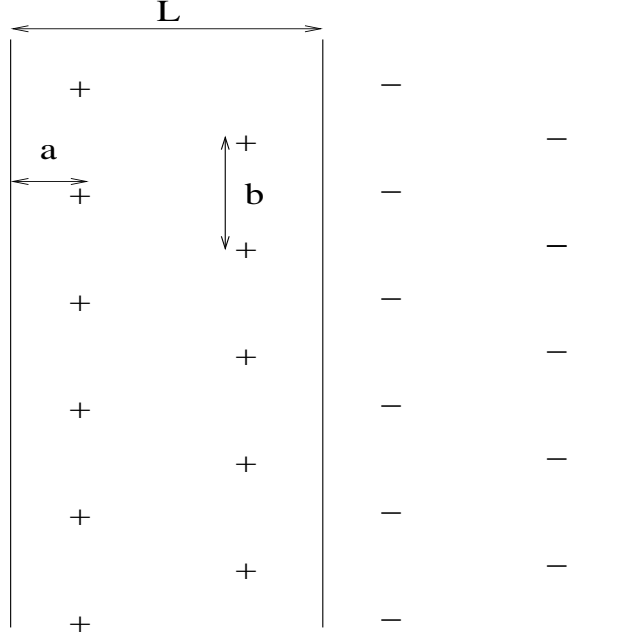


FIG. 5: The vortex lattice.

the lattices of discrete vortices only in the stripe phase, since the system favors that phase in equilibrium. In the continuum approximation, it is found that the vortex density increases at the closer distances to the magnetic domain walls. Based on this fact and the symmetry of the stripe domain structure, it is reasonable to consider that the vortices and antivortices form periodic structures on straight chains along the y direction. Even though it is not clear how many chains are associated with each domain, we can still make progress toward understanding discrete vortex lattices. In this section, we report our preliminary results on the problems; i) how the vortices and the antivortices are positioned on the chains; ii) how the equilibrium domain size changes, depending on the magnetization and the magnetic domain wall energy in the presence of the vortices. In order to solve these problems, we propose a configuration of the vortex and the antivortex chains in which two chains per stripe is considered. According to our results in the continuum regime, the vortex density increases near the domain walls. Therefore, we can have at least two chains per stripe in a possible configuration. Chains are situated at distance a from the magnetic domain walls. Another problem is how to place vortices and antivortices on the chains. If vortices are next to each other on the either side of the magnetic domain wall, the magnetic fields they produce cancel out each other. As a result, the gain in energy is diminished. However, the system has the largest gain when the vortices and antivortices are shifted by a half period $b/2$ (see Fig. 5).

Our next step is to write the energies of the proposed structure. To this end, we use (36,37,38). In those equations, the vortex configurations differ by their form-factors. We can obtain them from $F_{\mathbf{G}} = \sum_{\mathbf{r}_i} n_i e^{i\mathbf{G} \cdot \mathbf{r}_i}$, where the \mathbf{G} 's are the reciprocal vectors of the periodic structures, the \mathbf{r}_i are the positions of the vortex centers, and n_i are the charge of the vortex. In our proposed model, $\mathbf{G} = ((2r+1)\frac{\pi}{L}, 2s\frac{\pi}{b})$, $n_i = \pm 1$ and $F_{\mathbf{G}} = e^{iG_x a} - (-1)^s e^{-iG_x a}$. In our calcu-

lations, the divergent part of the series must be extracted carefully. We show below the detailed analysis of series equations for each candidate. We start with the self interaction energy of the magnetic layer U_{mm} , since it is the same for each configuration. For the periodic structures, it is given by (38). Direct substitution of the Fourier coefficient of the stripe phase $m_z \mathbf{G} = \frac{2im}{\pi(2r+1)}$ into Eq.(38) gives the self-interaction of the magnetic layer per unit cell as

$$u_{mm} = -\frac{8m^2}{L} \sum_{r=0}^{\infty} \frac{1}{\frac{L}{2\pi\lambda} + 2r + 1}. \quad (74)$$

This series is logarithmically divergent. However, it can be pulled out easily by adding and subtracting $1/(2r+1)$ in the series above. Thus, we get two terms; one convergent, the other divergent. Summing over r on the divergent part up to the cutoff $r_{max} = L/l$, where l is the magnetic domain wall width, we obtain the following:

$$u_{mm} = -\frac{4m^2}{L} \left(\ln \frac{L}{l} - \psi^{(0)} \left(\frac{1}{2} + \frac{L}{4\pi\lambda} \right) \right), \quad (75)$$

where $\psi^{(0)}(x)$ is the polygamma function of zeroth order [59]. In our numerical calculations, we write the logarithmic term in (75) as $\ln(\lambda/l) + \ln(L/\lambda)$ and then incorporate the $-4m^2 \ln(\lambda/l)$ term in the renormalized ϵ_{dw}^{ren} . Another energy term with a divergent series is the vortex energy, in general given by (36). The logarithmic divergence in this term stems from the vortex self-energies. We first split (36) into two parts as follows:

$$u_{vv} = \frac{\pi\epsilon_0}{2L^2b^2} \sum_{\mathbf{G}} \left[\frac{|F_{\mathbf{G}}|^2}{G^2} - \frac{|F_{\mathbf{G}}|^2}{G^2(1+2\lambda G)} \right]. \quad (76)$$

Note that the area of the elementary cell is $2Lb$. The first term of the series above contributes to the self-energies of the vortices; whereas, the second term is the vortex-vortex energy and will be left in the series form. The series in the first term can be transformed to the form of $\sum_{r=-\infty}^{\infty} \sum_{s=-\infty}^{\infty} 1/((2r+1)^2x^2 + s^2)$ where x is constant, and depends on the form-factor. A detailed analysis of such series is given in Appendix B.

The next step is to find the vortex energy and the interaction energy of the magnetization and vortices for each configuration. In the calculation of u_{mv} , we take the Fourier coefficient of the magnetization to be $\frac{4im}{(2r+1)}\delta(G_y)$. The fact that the stripe is infinite along the y direction results in the additional term $2\pi\delta(G_y)$. However, it does not play any role in the calculation of u_{mm} . For numerical analysis, these energies must be expressed in terms of dimensionless parameters. To this end, we define dimensionless variables $\tilde{\lambda} = \lambda/L$, $\tilde{b} = b/L$ and $\tilde{\epsilon}_{dw} = \epsilon_{dw}^{ren}\lambda/\epsilon_0$. The total energy \tilde{U} is measured in units of ϵ_0/λ^2 . In addition, we introduce the dimensionless magnetic energy as $\tilde{U}_{mm} = u_{mm}/(\epsilon_0/\lambda^2)$. In the fourth configuration, the square of the form-factor is: $|F_{\mathbf{G}}|^2 = 2 - 2(-1)^s \cos((2r+1)\pi\tilde{a})$. Even and odd values of s give different contributions. Then, we can calculate the vortex energy for even s and odd s separately. In terms of these parameters, we find

$$\tilde{U} = \frac{\tilde{\lambda}^2}{2\tilde{b}} \left(\ln \left(\frac{\lambda}{\tilde{\lambda}\tilde{\xi}} \right) - 2f_v(\tilde{\lambda}, \tilde{a}) - \frac{4}{\tilde{b}\pi} f_{vv}(\tilde{\lambda}, \tilde{a}, \tilde{b}) - \frac{16m\phi_0}{\epsilon_0} f_{mv}(\tilde{\lambda}) \right) + \tilde{U}_{mm} + \tilde{\epsilon}_{dw}\tilde{\lambda}, \quad (77)$$

where

$$\begin{aligned}
f_v &= \sum_{r=0}^{\infty} \frac{\coth((2r+1)\frac{\pi\tilde{b}}{4}) - 1}{2r+1} \sin^2((2r+1)\pi\tilde{a}) \\
&+ \sum_{r=0}^{\infty} \frac{\tanh((2r+1)\frac{\pi\tilde{b}}{4}) - 1}{2r+1} \sin^2((2r+1)\pi\tilde{a}), \\
f_{vv} &= \sum_{r,s=-\infty}^{\infty} \frac{\sin^2((2r+1)\pi\tilde{a})}{((2r+1)^2 + \frac{16s^2}{\tilde{b}^2})(1 + 2\pi\tilde{\lambda}\sqrt{(2r+1)^2 + \frac{16s^2}{\tilde{b}^2}})}, \\
&+ \sum_{r,s=-\infty}^{\infty} \frac{\cos^2((2r+1)\pi\tilde{a})}{((2r+1)^2 + \frac{4(2s+1)^2}{\tilde{b}^2})(1 + 2\pi\tilde{\lambda}\sqrt{(2r+1)^2 + \frac{4(2s+1)^2}{\tilde{b}^2}})}, \\
f_{mv} &= \sum_{r=0}^{\infty} \frac{\sin((2r+1)\pi\tilde{a})}{(2r+1)(1 + 2\pi\tilde{\lambda}(2r+1))}. \tag{78}
\end{aligned}$$

In the numerical minimization of Eq.(77), we take $\ln(\lambda/\xi) = 5$. Changing $m\phi_0/\varepsilon_0$ at fixed $\tilde{\varepsilon}_{dw}$, which initially is fixed at 0.5, we calculate the minimal energy of the proposed configuration. We first investigate when this configurations becomes energetically favorable in the system. To this end, we check where the equilibrium energies of the configuration first become negative.

TABLE I: The numerical results for the fourth configuration at $\tilde{\varepsilon}_{dw} = 0.5$. The column on the left is input.

$m\phi_0/\varepsilon_v$	L/λ	a/λ	b/λ
2.00	2.50	0.56	0.18
3.00	1.67	0.38	0.12

In numerical calculations, we also found that the vortex lattice is stable for $\varepsilon_{dw} > 4\tilde{m}^2$. At this point, the domain size is noticeably larger than the effective penetration depth λ , so the continuum approximation is valid. Therefore, we expect that the domain nucleation starts in the continuum regime. This problem is left for the future research. As seen in Table I, at constant $\tilde{\varepsilon}_{dw}$, with increasing $m\phi_0/\varepsilon_v$, the equilibrium size of the domain decreases. In addition, the vortices on the chain get closer to each other. These results agree with those obtained in the continuum approximation. As $\varepsilon_{dw}/4\tilde{m}^2$ increases, we expect that new vortex chains develop within the domains. We leave this problem to future research.

V. CONCLUSIONS

We reviewed theory of the heterogeneous magnetic superconducting systems (HMSS) based on London-Maxwell equations and the application of the theory on two realizations: ferromagnetic (FM) dots and their square array on a superconducting (SC) film, and ferromagnetic-superconducting bilayers (FSB). In the first chapter, we presented a general formalism for the

interaction between magnetic textures and superconductors in the Londons approximation. The problem is formulated as a variational principle. The variational functional (energy) is an integral over regions occupied either by magnet or by superconductor. It allows us to find directly the positions of vortices and magnetization. Afterwards, the formalism is extended to the case of periodic structures and finite systems.

As applications of the formalism, we have shown that vortices in superconducting films can be generated by magnetic dots magnetized normal to the film. We have found phase transition curves separating the state without vortices from the state with one vortex and the latter from the state with two vortices. Up to 7 vortices, the vortex-configurations on the ground state of a SC film with the FM dot on it are determined. For one vortex under a dot we have shown that the perpendicular component of magnetic field changes sign at some distance from the dot. This fact can be used for diagnostics of the vortex generation.

However, we treat only vortices under the FM dot. In a more realistic picture, the antivortices outside the dot become important and most likely affect the configurations of the vortices confined within the dot's region. This problem still remains open.

In the fourth chapter, we studied ferromagnetic-superconducting bilayers (FSB). We predicted that in a finite temperature interval below the SC transition the FSB is unstable with respect to SC vortex formation. The slow decay ($\propto 1/r$) of the long-range interactions between Pearl vortices makes the structure that consists of alternating domains with opposite magnetization and vorticity energetically favorable. The distribution of vortices inside each domain is highly inhomogeneous, with density increasing near the magnetic domain walls. As long as the domain width is larger than the effective penetration depth, the energy of the stripe domain structure is minimized. These new topological structures can be observed directly. A strong anisotropy in current transport would provide indirect evidence of the stripe texture: the bilayer may be superconducting for current parallel to the domains and resistive for current perpendicular to the domains.

If $\epsilon_{dw} \leq 4\tilde{m}^2$, the continuum approximation becomes invalid. Instead, we considered the discrete lattice of vortices. We analyzed the vortex configurations in two vortex chains. Depending on the magnetization and the magnetic domain wall energy, the positions of the vortices and the equilibrium domain size are calculated.

It is possible that the long domain nucleation time can interfere with the observation of described textures. We expect, however, that the vortices that appear first will reduce the barriers for domain walls and, subsequently, expedite domain nucleation. Quantitative study of this dynamic process is still in progress.

Our purpose was to consider quantitatively a new class of phenomena provided by the interaction between superconductivity and ferromagnetism in heterogeneous systems. This review article focuses on unusual equilibrium structures of vortices and magnetization occurring in such systems. As the simplest specific examples we considered single magnetic dots and also SC-FM bilayers. We have shown that, because of the numerous parameters for the system, such as temperature, magnetization, thickness etc., these systems display a complex phase diagram. We did not exhaust all possible states. Moreover, dynamic effects and transport properties are beyond the scope of this article. However, we believe that our primary results are of experimental interest and have technological promise.

We believe that the most experimentally interesting and challenging predictions are: (1), the existence of domain structures with alternating magnetization and vortex polarity in FM-SC bilayers and their shrinking below the SC transition temperature; (2), the formation of several

vortices under the magnetic dots placed on top of a SC film; (3), the symmetry violation in the periodic array of the magnetic dots on SC films. Although, antivortices outside the single magnetic dot are not analyzed in this article, they are expected to occur in real systems. All these effects can be observed directly by scanning tunnelling microscopy, scanning Hall probe microscopy and micro SQUID measurements.

In conclusion, our results not only confirm some old results found by means of different methods, but also present a class of new physical effects in HMSS. In this sense, they manifest a new direction and motivation for the possible experiments in the future.

APPENDIX A: THE PEARL VORTEX

The vortices in thin superconducting(SC) films are first studied by J. Pearl [29]. Here, we give the detailed calculations of vector potential and magnetic field for Pearl vortex located at \mathbf{r}_0 on the SC film. We start with the London-Pearl equation:

$$\nabla^2 \mathbf{A}(\mathbf{r}, z) = \frac{1}{\lambda} \mathbf{a}(\mathbf{r}) \delta(z) - \frac{\phi_0}{2\pi\lambda} \nabla \varphi(\mathbf{r} - \mathbf{r}_0) \delta(z), \quad (\text{A1})$$

where $\mathbf{a}(\mathbf{r}) = \mathbf{A}(\mathbf{r}, z = 0)$. It is easy to find the vector potential due to the vortex by employing the Fourier transformation to Eq.(A1). In doing so, we use

$$\mathbf{A}(\mathbf{r}, z) = \int \mathbf{A}_{\mathbf{k}} e^{i\mathbf{q} \cdot \mathbf{r} + ik_z z} \frac{d\mathbf{k}}{(2\pi)^3}. \quad (\text{A2})$$

In the Fourier representation, the London-Pearl equation reads

$$\mathbf{A}_{\mathbf{k}} = -\frac{1}{\lambda k^2} \mathbf{a}_{\mathbf{q}} + \frac{\phi_0}{2\pi\lambda} \frac{(\nabla \varphi)_{\mathbf{q}}}{k^2}, \quad (\text{A3})$$

where $(\nabla \varphi)_{\mathbf{q}} = 2\pi \frac{i\hat{q} \times \hat{z}}{q} e^{-i\mathbf{q} \cdot \mathbf{r}_0}$ [57]. Employing integral over k_z to Eq.(A3) and using $\mathbf{a}_{\mathbf{q}} = \int_{-\infty}^{\infty} \frac{dk_z}{2\pi} \mathbf{A}_{\mathbf{k}}$, we obtain the Fourier-transform of the vortex-induced vector potential at the SC film as

$$\mathbf{a}_{\mathbf{q}} = \frac{i\phi_0(\hat{q} \times \hat{z})e^{-i\mathbf{q} \cdot \mathbf{r}_0}}{q(1 + 2\lambda q)}. \quad (\text{A4})$$

Substituting the above equation in Eq.(A3), the 3d vortex-induced vector potential is found as

$$\mathbf{A}_{\mathbf{k}} = \frac{2i\phi_0(\hat{q} \times \hat{z})e^{-i\mathbf{q} \cdot \mathbf{r}_0}}{\mathbf{k}^2(1 + 2\lambda q)}. \quad (\text{A5})$$

The direct substitution of Eq.(A5) back in Eq.(A2) leads to

$$\mathbf{A}(\mathbf{r}, z) = \int \frac{2i\phi_0(\hat{q} \times \hat{z})e^{-i\mathbf{q} \cdot (\mathbf{r} - \mathbf{r}_0) + ik_z z}}{\mathbf{k}^2(1 + 2\lambda q)} \frac{d^2 q dk_z}{(2\pi)^3}. \quad (\text{A6})$$

First, we perform integral over k_z , and find

$$\mathbf{A}(\mathbf{r}, z) = \int \frac{i\phi_0(\hat{q} \times \hat{z})e^{-i\mathbf{q} \cdot (\mathbf{r} - \mathbf{r}_0)} e^{-q|z|}}{q(1 + 2\lambda q)} \frac{d^2 q}{(2\pi)^2}. \quad (\text{A7})$$

Let

$$\mathbf{q} = q \cos(\theta + \phi) \hat{u} + q \sin(\theta + \phi) \hat{v} \quad (\text{A8})$$

$$\mathbf{r} - \mathbf{r}_0 = |\mathbf{r} - \mathbf{r}_0| \cos \phi \hat{u} + |\mathbf{r} - \mathbf{r}_0| \sin \phi \hat{v}, \quad (\text{A9})$$

where \hat{u} and \hat{v} are unit vectors in a plane perpendicular to the z -direction, θ is the angle between \mathbf{q} and $\mathbf{r} - \mathbf{r}_0$, and ϕ is the angle between $\mathbf{r} - \mathbf{r}_0$ and \hat{u} . By (A8), $\hat{q} \times \hat{z}$ in Eq.(A7) reads

$$\hat{q} \times \hat{z} = -\cos(\theta + \phi) \hat{v} + \sin(\theta + \phi) \hat{u}. \quad (\text{A10})$$

Substituting (A10) in Eq.(A7), and using $\hat{u} \times \hat{z} = -\hat{v}$, $\hat{v} \times \hat{z} = \hat{u}$, $\int_0^{2\pi} e^{ix \cos \theta} \cos \theta d\theta = 2\pi i J_1(x)$ and $\int_0^{2\pi} e^{ix \cos \theta} \sin \theta d\theta = 0$, we find

$$\mathbf{A}(\mathbf{r}, z) = \frac{n\phi_0}{2\pi} \frac{\hat{z} \times (\mathbf{r} - \mathbf{r}_0)}{|\mathbf{r} - \mathbf{r}_0|} \int_0^\infty \frac{J_1(q|\mathbf{r} - \mathbf{r}_0|) e^{-q|z|}}{1 + 2\lambda q} dq. \quad (\text{A11})$$

Note that in the above equation, $\cos \phi \hat{v} - \sin \phi \hat{u} = \frac{\hat{z} \times (\mathbf{r} - \mathbf{r}_0)}{|\mathbf{r} - \mathbf{r}_0|}$. From $\mathbf{B} = \nabla \times \mathbf{A}$, the magnetic field components of the Pearl vortex are found as follows:

$$B_r(\mathbf{r}, z) = \frac{n\phi_0}{2\pi} \text{sign}(z) \int_0^\infty \frac{J_1(q|\mathbf{r} - \mathbf{r}_0|) q e^{-q|z|}}{1 + 2\lambda q} dq, \quad (\text{A12})$$

$$B_z(\mathbf{r}, z) = \frac{n\phi_0}{2\pi} \int_0^\infty \frac{J_0(q|\mathbf{r} - \mathbf{r}_0|) q e^{-q|z|}}{1 + 2\lambda q} dq. \quad (\text{A13})$$

APPENDIX B: INTEGRALS OF BESSEL FUNCTIONS

In this appendix, the asymptotic values and the exact results of the Bessel integrals used in this article are introduced. First, we present the integrals containing one Bessel function. These integrals are in the form of

$$\int_0^\infty \frac{J_m(kr) k^n}{1 + 2k\lambda} dk, \quad (\text{B1})$$

where $m = 0, 1$ and $n = 0, 1$. For $m = 0, 1$ and $n = 0$, the exact results can be obtained as follows [64]:

$$\int_0^\infty \frac{J_0(kr)}{1 + 2\lambda k} dk = \frac{\pi}{4\lambda} [H_0\left(\frac{r}{2\lambda}\right) - Y_0\left(\frac{r}{2\lambda}\right)], \quad (\text{B2})$$

$$\int_0^\infty \frac{J_1(kr)}{1 + 2\lambda k} dk = \frac{\pi}{4\lambda} [H_{-1}\left(\frac{r}{2\lambda}\right) + Y_1\left(\frac{r}{2\lambda}\right)] + \frac{1}{r}, \quad (\text{B3})$$

where $H_l(x)$ and $Y_l(x)$ are the Struve function and the second kind of the Bessel function of the l th order [59]. The respective asymptotic values of Eqs.(B2, B3) are found as follows: When $r \ll \lambda$, which corresponds to $k\lambda \gg 1$, the integral in (B2) becomes [65]

$$\int_0^\infty \frac{J_0(kr)}{2k\lambda} dk = \frac{1}{2\lambda} [\ln\left(\frac{\lambda}{r}\right) - C]. \quad (\text{B4})$$

For $r \gg \lambda$, which is equivalent to $k\lambda \ll 1$, the integral in (B2) becomes [65]

$$\int_0^\infty J_0(kr)dk = \frac{1}{r}. \quad (\text{B5})$$

Using the same techniques, the asymptotic values of the integral in (B3) are

$$\int_0^\infty \frac{J_1(kr)}{1+2k\lambda}dk \approx \int_0^\infty \frac{J_1(kr)}{2k\lambda}dk = \frac{1}{2\lambda} \quad r \ll \lambda \quad (\text{B6})$$

$$\int_0^\infty \frac{J_1(kr)}{1+2k\lambda}dk \approx \int_0^\infty J_1(kr)dk = \frac{1}{r} \quad r \gg \lambda. \quad (\text{B7})$$

In order to find the asymptotic values for $m = 0, 1$ and $n = 1$, we use

$$\int_0^\infty J_m(kr)k^n dk = \lim_{\alpha \rightarrow 0} \frac{\partial^n}{\partial \alpha^n} \int_0^\infty J_m(kr)e^{-\alpha k} dk. \quad (\text{B8})$$

With similar techniques and (B8), the asymptotic values are given as follows:

$$\int_0^\infty \frac{J_0(kr)}{1+2k\lambda}kdk \approx \int_0^\infty \frac{J_0(kr)}{2\lambda}dk = \frac{1}{2\lambda r} \quad r \ll \lambda. \quad (\text{B9})$$

For $r \gg \lambda$, the integral becomes $\int_0^\infty J_0(kr)kdk$, which equals zero [65]. In order to find nonzero result, we do the following approximation: $r \gg \lambda$ is equivalent to $k\lambda \ll 1$. Therefore, the fraction in (B1) can be rewritten as

$$\frac{1}{1+2k\lambda} = 1 - 2k\lambda + \dots \quad (\text{B10})$$

By (B10), we obtain

$$\int_0^\infty \frac{J_0(kr)}{1+2k\lambda}kdk \approx -2\lambda \int_0^\infty J_0(kr)k^2 dk = \frac{2\lambda}{r^3} \quad r \gg \lambda, \quad (\text{B11})$$

and,

$$\int_0^\infty \frac{J_1(kr)}{1+2k\lambda}kdk \approx \int_0^\infty \frac{J_1(kr)}{2\lambda}dk = \frac{1}{2\lambda r} \quad r \ll \lambda \quad (\text{B12})$$

$$\int_0^\infty \frac{J_1(kr)}{1+2k\lambda}kdk \approx \int_0^\infty J_1(kr)kdk = \frac{1}{r^2} \quad r \gg \lambda. \quad (\text{B13})$$

We give only the asymptotic values of the integrals with two Bessel functions. We start with the following integral:

$$\int_0^\infty \frac{J_1(kR)J_0(kr)}{1+2k\lambda}dk. \quad (\text{B14})$$

For the above integral, we first analyze the case, in which $R \ll \lambda$. In this case, we can replace $J_1(kR)$ by $kR/2$ in (B14). In doing so, we get

$$\int_0^\infty \frac{J_1(kR)J_0(kr)}{1+2k\lambda}dk \approx \frac{R}{2} \int_0^\infty \frac{J_0(kr)}{1+2k\lambda}kdk. \quad (\text{B15})$$

Using the asymptotic values for the integral on the left in (B9) and (B11), we find

$$\int_0^\infty \frac{J_1(kR)J_0(kr)}{1+2k\lambda} dk = \frac{R}{4\lambda r} \quad R \ll r \ll \lambda \quad (\text{B16})$$

$$= \frac{2\lambda R}{r^3} \quad R \ll \lambda \ll r. \quad (\text{B17})$$

For $R > \lambda$ and $r > \lambda$, we can neglect $2k\lambda$ in Eq.(B14). In doing so, we obtain

$$\int_0^\infty \frac{J_1(kR)J_0(kr)}{1+2k\lambda} dk \approx \int_0^\infty J_1(kR)J_0(kr) dk. \quad (\text{B18})$$

The above integral equals [65]

$$\int_0^\infty J_1(kR)J_0(kr) dk = 0 \quad R < r \quad (\text{B19})$$

$$= \frac{1}{2R} \quad R = r \quad (\text{B20})$$

$$= \frac{1}{R} \quad r < R. \quad (\text{B21})$$

The other integral of interest containing two Bessel functions is

$$\int_0^\infty \frac{J_1(kR)J_0(kr)k^2}{1+2k\lambda} dk. \quad (\text{B22})$$

For $R < \lambda$, using $J_1(kR) \approx kR/2$, the integral in Eq.(B22) becomes

$$\frac{R}{2} \int_0^\infty \frac{J_0(kr)k^3}{1+2k\lambda} dk. \quad (\text{B23})$$

By (B8) and (B10), the asymptotic values of the above integral can be calculated as follows: for $r \ll \lambda$, (B22) can be rewritten as

$$\frac{R}{4\lambda} \int_0^\infty J_0(kr)k^2 dk = \frac{R}{4\lambda r^3}. \quad (\text{B24})$$

For $R \ll r$, (B23) becomes

$$-R\lambda \int_0^\infty J_0(kr)k^4 dk = -\frac{9R\lambda}{r^5}. \quad (\text{B25})$$

Now, we can write the asymptotic values of (B22) as

$$\int_0^\infty \frac{J_1(kR)J_0(kr)k^2}{1+2k\lambda} dk \approx \frac{R}{4\lambda r^3} \quad R \ll r \ll \lambda \quad (\text{B26})$$

$$\int_0^\infty \frac{J_1(kR)J_0(kr)k^2}{1+2k\lambda} dk \approx -\frac{9R\lambda}{r^5}. \quad R \ll \lambda \ll r. \quad (\text{B27})$$

APPENDIX C: CALCULATION OF SERIES

In this appendix, the detailed analysis of series is given. First, the series in the energy calculations of the periodic systems are analyzed; second, the detailed calculation of the vortex density is shown. The series we encounter in the energy calculations fall into two categories. In the first category, we sum over one variable. The series in this category are in the form of $\sum_{r=1}^{r_{max}} 1/r$. Employing the Euler-Maclaurin summation formula [66], the summation is found with logarithmic accuracy as

$$\sum_{r=1}^{r_{max}} \frac{1}{r} \approx \ln r_{max} + C. \quad (C1)$$

where $C \sim 0.577$ is the Euler-Mascheroni constant. If the summation is performed over only odd integers, we can still transform our series to (C1). Namely,

$$\sum_{r=0}^{r_{max}} \frac{1}{2r+1} \approx \sum_{r=1}^{2r_{max}+1} \frac{1}{r} - \frac{1}{2} \sum_{r=1}^{r_{max}/2} \frac{1}{r}, \quad (C2)$$

$$\approx \ln(2r_{max}+1) + C - \ln\left(\frac{r_{max}}{2}\right) - \frac{C}{2}, \quad (C3)$$

$$\approx \frac{1}{2}(\ln r_{max} + C + 2\ln 2). \quad (C4)$$

The second category is the double series. In this aspect, we first show the calculation of square domain energy in the continuum approximation. The corresponding energy contains the series

$$S = \sum_{r,s=0}^{\infty} \frac{\sqrt{(2r+1)^2 + (2s+1)^2}}{(2r+1)^2(2s+1)^2}. \quad (C5)$$

Our goal is to calculate the logarithmic contribution due to the self-vortex energies and the constant as a next approximation. The sum in (C5) diverges logarithmically in two regions: $r \gg s$ and $s \gg r$. Keeping this in mind, (C5) can be rewritten as

$$S = \sum_{r,s=-\infty}^{\infty} \frac{\max(2r+1, 2s+1)}{(2r+1)^2(2s+1)^2} + \sum_{r,s=-\infty}^{\infty} \frac{\sqrt{(2r+1)^2 + (2s+1)^2} - \max(2r+1, 2s+1)}{(2r+1)^2(2s+1)^2}. \quad (C6)$$

The first term in the above series contributes the logarithmic term S_{log} , and here it is

$$S_{log} = 2 \sum_{r_{max}} \frac{1}{2r+1} \sum_{s=0}^{\infty} \frac{1}{(2s+1)^2} \quad (C7)$$

$$\approx \frac{\pi^2}{8}(\ln r_{max} + C + 2\ln 2). \quad (C8)$$

We used the result in Eq.(C4), and $\sum_{s=0}^{\infty} \frac{1}{(2s+1)^2} = \frac{\pi^2}{8}$ [67]. The other term in (C6) contributes the constant S_{cons} . For three regions $r = s$, $r > s$ and $s > r$, the second series in (C6) is rewritten as follows:

$$S_{cons} = (\sqrt{2} - 2) \sum_{r=0}^{\infty} \frac{1}{(2r+1)^3} + 2 \sum_{r=0}^{\infty} \sum_{s=r+1}^{\infty} \frac{\sqrt{(2r+1)^2 + (2s+1)^2} - (2r+2s+2)}{(2r+1)^2(2s+1)^2}. \quad (C9)$$

Numerical calculation gives $S_{cons} = -1.19$.

The other double series of interest here are in the form of

$$I(x) = \sum_{r=-\infty}^{r=\infty} \sum_{s=-\infty}^{s=\infty} \frac{1}{x^2 r^2 + s^2}, \quad (C10)$$

where x is an arbitrary constant. Although (C10) is logarithmically divergent, the sum over one of the variables can be done easily. To this end, we perform the sum over s first. In doing so, Eq. (C10) becomes $(2\pi/x) \sum_{r=1}^{\infty} \coth(\pi x r)/r$ [67]. This series is logarithmically divergent. In order to get the logarithmic term, we add and subtract $1/r$. Using the result in (C1), finally we get

$$I(x) \approx \frac{2\pi}{x} \left[\sum_{r=1}^{\infty} \frac{\coth(\pi x r) - 1}{r} + \ln r_{max} + C \right]. \quad (C11)$$

Employing the same techniques, we give the results of the different versions of Eq. (C10) below:

$$\sum_{r=-\infty}^{r=\infty} \sum_{s=-\infty}^{s=\infty} \frac{1}{x^2(2r+1)^2 + s^2} \approx \frac{2\pi}{x} \left[\sum_{r=0}^{\infty} \frac{\coth((2r+1)\pi x) - 1}{2r+1} + \frac{\ln r_{max}}{2} + \frac{C}{2} \right], \quad (C12)$$

$$\sum_{r=-\infty}^{r=\infty} \sum_{s=-\infty}^{s=\infty} \frac{1}{x^2(2r+1)^2 + (2s+1)^2} \approx \frac{\pi}{x} \left[\sum_{r=0}^{\infty} \frac{\tanh((2r+1)\frac{\pi x}{2}) - 1}{2r+1} + \frac{\ln r_{max}}{2} + \frac{C}{2} \right]. \quad (C13)$$

In (C12) and (C13), we use $\sum_{s=0}^{\infty} 1/(y^2 + (2s+1)^2) = \pi \tanh(\pi y/2)/(4y)$. In the presence of $\sin^2((2r+1)y)$ or $\cos^2((2r+1)y)$, the series can be calculated in a similar way, using $\sin^2((2r+1)y) = (1 - \cos(2(2r+1)y))/2$ or $\cos^2((2r+1)y) = (1 + \cos(2(2r+1)y))/2$. For example,

$$\begin{aligned} \sum_{r=-\infty}^{r=\infty} \sum_{s=-\infty}^{s=\infty} \frac{\sin^2((2r+1)y)}{(x^2(2r+1)^2 + s^2)} &= \frac{2\pi}{x} \left[\sum_{r=0}^{\infty} \frac{\sin^2((2r+1)y)(\coth((2r+1)\pi x) - 1)}{2r+1} \right. \\ &\quad \left. + \frac{\ln r_{max}}{4} - \frac{\ln |\cot(y/2)|}{4} + \frac{C}{4} \right], \end{aligned} \quad (C14)$$

$$\begin{aligned} \sum_{r=-\infty}^{r=\infty} \sum_{s=-\infty}^{s=\infty} \frac{\cos^2((2r+1)y)}{(x^2(2r+1)^2 + s^2)} &= \frac{2\pi}{x} \left[\sum_{r=0}^{\infty} \frac{\sin^2((2r+1)y)(\coth((2r+1)\pi x) - 1)}{2r+1} \right. \\ &\quad \left. + \frac{\ln r_{max}}{4} + \frac{\ln |\cot(y/2)|}{4} + \frac{C}{4} \right]. \end{aligned} \quad (C15)$$

We use

$$\sum_{r=0}^{\infty} \frac{\cos((2r+1)\theta)}{2r+1} = \frac{\ln|\cot(\theta/2)|}{2}. \quad (\text{C16})$$

The Fourier transform of the vortex density $n_{\mathbf{G}}$ for the stripe domain structure is found by substituting the corresponding reciprocal lattice vectors $G = \pi(2r+1)/L$ and the Fourier transform of the step function $s_{\mathbf{G}} = \frac{2i}{\pi(2r+1)}$ in Eq.(64). In doing so, we obtain

$$n_{\mathbf{G}} = -\frac{4\pi i \tilde{\epsilon}_v}{L\phi_0^2} \sum_{r=-\infty}^{\infty} \text{sign}(2r+1). \quad (\text{C17})$$

Employing the inverse Fourier transform to Eq.(C17) gives the following series:

$$F(x) = \sum_{r=-\infty}^{\infty} \text{sign}(2r+1) e^{i(2r+1)\frac{\pi x}{L}} = 2i \sum_{r=0}^{\infty} \sin((2r+1)\frac{\pi x}{L}). \quad (\text{C18})$$

In order to calculate the above series, we integrate both sides over x . In doing so, by (C16) we find

$$\int F(x) dx = -2i \frac{L}{\pi} \sum_{r=0}^{\infty} \frac{\cos((2r+1)\frac{\pi x}{L})}{2r+1} = -i \frac{L}{\pi} \ln|\cot(\frac{\pi x}{2L})|. \quad (\text{C19})$$

The derivative of the above equation with respect to x gives

$$F(x) = -\frac{i}{\sin(\frac{\pi x}{L})}. \quad (\text{C20})$$

By (C17) and (C20), the vortex density $n(x)$ becomes

$$n(x) = -\frac{4\pi \tilde{\epsilon}_v}{L\phi_0^2} \frac{1}{\sin(\frac{\pi x}{L})}. \quad (\text{C21})$$

IV. REFERENCES

- [1] I.F. Lyuksyutov and V.L. Pokrovsky, Phys. Rev. Lett. **81**, (1998) 2344.
- [2] I.F. Lyuksyutov and V.L. Pokrovsky, *Superconducting Superlattices II: Native and Artificial*, Vol. 3480 (Eds. Ivan Bozovic and Davor Pavuna), SPIE-International Society for Optical Engineering, Bellingham, WA, (1998), pp. 230.
- [3] L.N. Bulaevskii, A.I. Buzdin, M.L. Kubic and S.V. Panyukov, Adv. Phys. **34**, (1985) 175.
- [4] O. Fisher, *Magnetic Superconductors*, Vol. 5 (Eds. K.H.J. Buschow and E.P. Wohlfarth), North-Holland, Amsterdam, (1990), pp. 465.
- [5] M. Belic and M.V. Jaric, Phys. Rev. Lett. **42**, (1979) 1015.
- [6] H.S. Greenside, E.I. Blount and C.M. Varma, Phys. Rev. Lett. **46**,(1981) 49.
- [7] V.L. Ginzburg, Zh. E'ksp. Teor. Fiz. **31**, (1957) 202 [Sov. Phys. JETP **4**,(1957) 153].
- [8] P.W. Anderson and H. Suhl, Phys. Rev. **116**, (1959) 898.
- [9] P. Fulde and R.A. Ferrell, Phys. Rev. **135**, (1964) 550.
- [10] A.I. Larkin and Yu.N. Ovchinnikov, Zh. E'ksp. Teor. Fiz. **47**, (1964) 1136 [Sov. Phys. JETP **20**, (1965) 762].
- [11] H. Suhl, J. Less-Common Metals **62**, (1978) 225.
- [12] B.T. Mathias, H. Suhl and E. Corenzwit, Phys. Rev. Lett. **1**, (1958) 92.
- [13] C. Bernhard, J.L. Tallon, Ch. Niedermayer, Th. Blasius, A. Golnik, E. Brucher, R.K. Kremer, D.R. Noakes, C.E. Stronach and E.J. Ansaldo, Phys. Rev. B **59**, (1999) 14099.
- [14] L. Bauernfeind, W. Widder and H. Braun, *Fourth Euro Ceramics*, Vol. 6 Faenza Editrice S.p.A., Italy, (1995).
- [15] I. Felner, U. Asaf, Y. Levi and O. Millo, Phys. Rev. B **55**, (1997) R3374.
- [16] S. Erdin, Physica C **391**,(2003) 140.
- [17] I.K. Marmoros, A. Matulis and F.M. Peeters, Phys. Rev. B **53**,(1996) 2677.
- [18] M. A. Kayali, Phys. Lett. A, **298**, (2002) 432.
- [19] M. A. Kayali, Phys. Rev. B, **69**, (2004) 012505.
- [20] I.F. Lyuksyutov and V.L. Pokrovsky, cond-mat/9903312 (unpublished).
- [21] S.Erdin, I.F. Lyuksyutov, V.L. Pokrovsky and V.M. Vinokur, Phys. Rev. Lett. **88**, (2002) 017001.
- [22] M.A. Kayali and V.L. Pokrovsky, Phys. Rev. B **69**, (2004) 132501.
- [23] V.L. Pokrovsky and H. Wei, Phys. Rev. B **69**, (2004) 104530.
- [24] I.F. Lyuksyutov and D.G. Naugle, Modern Phys. Lett. B **13**, (1999) 491.
- [25] I.F. Lyuksyutov and D.G. Naugle, Int. J. Mod. Phys. B **17**, (2003) 3713.
- [26] S. Erdin, in press Phys. Rev. B **69** (2004).
- [27] S.Erdin, A.M. Kayali, I.F. Lyuksyutov and V.L. Pokrovsky, Phys.Rev.B **66**, (2002) 014414.
- [28] E.H. Brandt, Rep. Prog. Phys. **58**, (1995) 1465.
- [29] J. Pearl, Appl. Phys. Lett. **5**, (1964) 65.
- [30] M.V. Milosovic and F.M. Peeters, Phys. Rev. B **69**, (2004) 104522.
- [31] J.E. Santos, E. Frey and F. Schwabl, Phys. Rev. B **63** (2001) 4439.
- [32] R. Sasik and T. Hwa, cond-mat/0003462 (unpublished).
- [33] G. Carneiro, Physica C **404**, (2004) 78.

- [34] D.J. Priour Jr. and H.A. Fertig, *Physica C* **404**, (2004) 293.
- [35] L.N. Bulaevskii, E.M. Chudnovsky and M.P. Maley, *Appl. Phys. Lett.* **76**, (2000) 2594.
- [36] L.N. Bulaevskii and E.M. Chudnovsky, *Phys. Rev. B* **63** (2001) 2502.
- [37] L.E. Helseth, *Phys. Lett. A*, Vol.315, (2003) 399.
- [38] J.I. Martin, M. Velez, J. Nogues and I.K. Schuller, *Phys.Rev. Lett.* **79**, (1997) 1929.
- [39] D.J. Morgan and J.B. Ketterson *Phys. Rev. Lett.* **80**, (1998) 3614.
- [40] Y. Otani, B. Pannetier, J.P. Nozieres and D. Givord, *J. Magn. Mag. Mat.* **126**, (1993) 622.
- [41] O. Geoffroy, D. Givord, Y. Otani, B. Pannetier and F. Ossart, *J. Magn. Mag. Met.* **121**, (1993) 223.
- [42] Y. Nozaki, Y. Otani, K. Runge, H. Miyajima, B. Pannetier, J.P. Nozieres and G. Fillion, *J. Appl. Phys.* **79**, (1996) 8571.
- [43] M.J. Van Bael, L. Van Look, K. Temst, M. Lange, J. Bekaert, U. May, G. Guntherodt, V.V. Moshchalkov and Y. Bruynseraede, *Physica C* **332**, (2000) 12.
- [44] A. Terentiev, D.B. Watkins, L.E. De Long, D.J. Morgan and J.B. Ketterson, *Physica C* **332**, (2000) 5.
- [45] M.J. Van Bael, K. Temst, V.V. Moshchalkov and Y. Bruynseraede, *Phys. Rev. B* **59**, (1999) 14674.
- [46] P.Martinoli, N. Nsabimana, G.A. Racine, H. Beck and R. Clem, *Helv. Phys. Acta.* **56**, (1983) 765.
- [47] V.V. Metlushko, M. Baert, R. Jonckheere, V.V. Moshchalkov and Y. Bruynseraede, *Solid State Comm.* **91**, (1994) 331.
- [48] M. Baert, V.V. Metlushko, R. Jonckheere, V.V. Moshchalkov and Y. Bruynseraede *Phys. Rev. Lett.* **74**, (1995) 3269.
- [49] V.V. Moshchalkov, M. Baert, V.V. Metlushko, E. Rosseel, M.J. VanBael, K. Temst, R. Jonckheere and Y. Bruynseraede *Phys. Rev. B* **54**, (1996) 7385.
- [50] V.V. Metlushko, L.E. DeLong, M. Baert, E. Rosseel, M.J. VanBael, K. Temst, R. Jonckheere and Y. Bruynseraede, *Europhys. Lett.* **41**, (1998) 333.
- [51] I.F. Lyuksyutov and D.G. Naugle, *Physica C* **341**, (2000) 1267.
- [52] I.F. Lyuksyutov, D.G. Naugle and V.L. Pokrovsky, *Superconducting and Related Oxides: Physics and Nanoengineering IV*, Vol. 4058 (Eds. Davor Pavuna and Ivan Bozovic), SPIE-International Society for Optical Engineering, Bellingham, WA, (2000), pp. 376.
- [53] I.F. Lyuksyutov and V.L. Pokrovsky, *Modern. Phys. Lett.* **14**, (2000) 409.
- [54] L.E. Helseth, P.E. Goa, H. Hauglin, M. Baziljevich and T. Johansen, *Phys. Rev. B* **65**, (2002) 132514.
- [55] P.G. de Gennes, *Superconductivity of Metals and Alloys*, Addison-Wesley, (1989).
- [56] L.D. Landau and E.M. Lifshitz, *Electrodynamics of Continuous Media*, Butterworth-Heinemann, (1995), 2nd ed.
- [57] A.A. Abrikosov, *Introduction to the Theory of Metals* North Holland, (1986).
- [58] V.G. Kogan, *Phys. Rev. B* **49**, (1994) 15874.
- [59] M. Abramowitz and I. A. Stegun, *Handbook of Mathematical Functions*, Dover Publications, (1970).
- [60] A.P. Malozemoff and J.C. Slonczewski, *Magnetic Domain Walls in Bubble Materials*, Academic Press, (1979).
- [61] Y. Yafet and E.M. Gyorgy, *Phys. Rev. B* **38**, (1988) 9145.
- [62] A. Kashuba and V.L. Pokrovsky, *Phys. Rev. B* **48**, (1993) 10335.
- [63] A. Abanov, V. Kalatsky, V.L. Pokrovsky, W.M. Saslow, *Phys. Rev. B* **51**, (1995) 1023.
- [64] Y.L. Luke, *Integrals of Bessel Functions*, McGraw-Hill, (1962).

- [65] I.S. Gradshteyn and I.M. Ryzhik, *Tables of Integrals, Sums, Series and Products*, Academic Press, (1994), 5th ed.
- [66] G.B. Arfken and H.J. Weber, *Mathematical Methods for Physicists*, Academic Press, (2000), 5th ed.
- [67] E.R. Hansen, *A Table of Series and Products*, Prentice-Hall, (1975).